AFOSR-TR-95

0558

REPORT DOCUMENTATION PAGE

1. AGENCY USE ONLY (Leave blank)	2. REPORT DATE	3. REPORT TYPE AND DATES COVERED
		FINAL REPORT 01 Oct 93 - 30 Sep 94

4. TITLE AND SUBTITLE
Computer Simulations of Radiation Generation From Relativistic Electron Beams

5. FUNDING NUMBERS
61102F
2301/ES

6. AUTHOR(S)
Dr Anthony T. Lin

7. PERFORMING ORGANIZATION NAME(S) AND ADDRESS(ES)
Department of Physics
University of California, Los Angeles
Los Angeles, CA 90024-1547

8. PERFORMING ORGANIZATION REPORT NUMBER

9. SPONSORING/MONITORING AGENCY NAME(S) AND ADDRESS(ES)
AFOSR/NE
110 Duncan Avenue Suite B115
Bolling AFB DC 20332-0001

10. SPONSORING/MONITORING AGENCY REPORT NUMBER
F49620-93-1-0628

11. SUPPLEMENTARY NOTES

12a. DISTRIBUTION/AVAILABILITY STATEMENT
APPROVED FOR PUBLIC RELEASE: DISTRIBUTION UNLIMITED

12b. DISTRIBUTION CODE

13. ABSTRACT *(Maximum 200 words)*

SEE FINAL REPORT ABSTRACT

14. SUBJECT TERMS

15. NUMBER OF PAGES

16. PRICE CODE

17. SECURITY CLASSIFICATION OF REPORT	18. SECURITY CLASSIFICATION OF THIS PAGE	19. SECURITY CLASSIFICATION OF ABSTRACT	20. LIMITATION OF ABSTRACT
UNCLASSIFIED	UNCLASSIFIED	UNCLASSIFIED	UNCLASSIFIED

Institute of Plasma and Fusion Research

R F49620-93-1-0628 Final Technical Rep

Dr. Anthony T. Lin

UCLA Physics Department

Affiliated with the Departments of:

Astronomy
Earth and Space Sciences
Electrical Engineering
Materials Science and Engineering
Mechanical, Aerospace and Nuclear Engineering
Physics

and

Center for Advanced Accelerators
Institute of Geophysics and Planetary Physics

Computer Simulations of Radiation Generation From Relativistic Electron Beams

AFOSR F49620-93-1-0628 Final Technical Report

Dr. Anthony T. Lin

UCLA Physics Department

University of California, Los Angeles

Department of Physics

Los Angeles, CA 90024-1547

COMPUTER SIMULATIONS OF RADIATION GENERATION FROM RELATIVISTIC ELECTRON BEAMS

AFOSR F49620-93-1-0628

FINAL TECHNICAL REPORT

TO

AIR FORCE OFFICE OF SCIENTIFIC RESEARCH

Dr. Anthony T. Lin

Department of Physics
University of California, Los Angeles
Los Angeles, CA 90024-1547

October 1, 1993, to September 30, 1994

TABLE OF CONTENTS

I. Introduction

This is the Final Technical Report on work performed under the support of the Air Force Office of Scientific Research under Grant AFOSR F49620-93-1-0628 for the period October 1, 1993 to September 30, 1994. The objective of this work was to carry out basic physics research on the generation of coherent, tunable radiation from relativistic electron beams and exploring means of improving performances.

II. Summary of Work Accomplished

This work covered computer simulations and theoretical studies of radiation generation in free electron microwave devices. During the past fiscal year, we have carried out computer simulations and theoretical analyses to address various issues concerned with peniotron oscillators.

We propose to utilize the helical beam which is a natural beam formation from a helical wiggler for peniotron interaction. In the medium beam energy regime ($V \approx 200kV$), the advantage of a helical peniotron in comparison with a conventional peniotron is very significant. The latter interaction tends to increase the beam longitudinal energy while the former interaction converts both the transverse and longitudinal beam energy into wave energy. As a result the difference in overall efficiency can be as large as a factor of two.

In a vaned waveguide the difference in the frequency of adjacent transverse modes is small. As a consequence there is an uncertainty in interpretating experimental results to determine whether the output wave comes from the peniotron or gyrotron interaction. Our simulation results reveal that in the nonlinear regime, the peniotron interaction is always able to suppress the gyrotron interaction. This is due to the fact that the gyrotron interaction is a resonant interaction which induces only guiding center spread but no guiding center drift. Therefore the effect of a saturated

gyrotron mode on the peniotron interaction is to reduce its growth rate but not its efficiency.

Simulation results also show that a sustainable pulsating mode in peniotron backward wave oscillations can be excited if parameters are properly chosen, such that at some instant of time the reduction in beam energy resulting from the electron-wave interaction is to such an extent that its cyclotron harmonic line intersects with the wave guide dispersion curve in the positive k_z region. The generation of the forward traveling self-oscillating mode eliminates the residual backward traveling wave, which is very essential in establishing the relaxation oscillation.

Below we summarize the scope and main findings of these investigations. More detailed information are contained in the appended reports.

A. Helical Peniotron Oscillators

The recent advance in the technology of generating an axis-encircling beam has arisen a renew interest in investigating the feasibility of building peniotron devices. The basic mechanism which gives rise to the peniotron interaction is the electron guiding center $\vec{E}_{wave} \times B_0\hat{z}$ drift in an electronmagnetic wave field with a positive radial gradient. This drifting motion tends to make it possible that every electron is able to find its own favorable phase relative to the electromagnetic wave such that all electrons on the average are in a stronger RF field region during the decelerating phase and in a weaker RF field region during the accelerating phase. As a result, all electrons regardless of their initial phases lose energy to the wave which makes the peniotron interaction inherently a high efficiency device. From the past theoretical evaluation, a consensus has been reached that the essential elements for peniotron interaction are the vaned waveguide to provide the positive radial field gradient and an axis-encircling beam to maximize the initial electron-wave coupling.

In a conventional peniotron interaction, electron phases initially are uniformly distributed with respect to the electromagnetic wave. Here, we have investigated the feasibility of making use of a helical beam produced by a combined solenoidal and wiggler magnetic field which can be expressed in the cylindrical coordinates (r,θ,z) by

$$\underset{\sim}{B} = B_0\, e_z + 2B_w \left[I'_1 (k_w r) \cos(\theta - k_w z)\, e_r - \frac{I_1(k_w r)}{k_w r} \sin(\theta - k_w z)\, e_\theta + I_1(k_w r) \sin(\theta - k_w z)\, e_z \right], \qquad (1)$$

where $k_w = 2\pi / \lambda_w$, I_n is the modified Bessel function of the first kind, and I'_n is its derivative.

The equilibrium orbit of an electron in a combined solenoidal and wiggler field has been extensively studied in microwave free electron lasers. Its transverse velocity can be expressed as

$$\vec{v}_\perp = v_{\perp 0} \left[\cos(\bar{\Omega}_{||} t + \varphi_0)\, \hat{e}_x + \sin(\bar{\Omega}_{||} t + \varphi_0)\, \hat{e}_y \right] - \sum_{n=-\infty}^{\infty} v_{\perp n} \hat{e}_z \times \left[\sin(n k_w \bar{v}_{||} t) \hat{e}_x - \cos(n k_w \bar{v}_{||} t) \hat{e}_y \right], \qquad (2)$$

where

$$v_{\perp n} = \frac{2n\Omega_w \bar{v}_{||}}{k_w r_b (n k_w \bar{v}_{||} - \bar{\Omega}_{||})} I_n(k_w r_b) I_{n-1}(k_w r_g) \ .$$

The first term on the right-hand side of Eq.(2) is a general solution representing the conventional cyclotron oscillation. Its amplitude $v_{\perp 0}$ and phase φ_0 depend on the entrance conditions of the electron. It becomes negligible under adiabatic entrance conditions. Ω_w and $\bar{\Omega}_{||}$ are respectively the relativistic electron cyclotron frequency for wiggler and longitudinal fields and $\bar{\Omega}_{||} = B_0 + 2B_w I_1(k_w r_b) I_0(k_w r_g)$.

In the case of axis-encircling motion (r_g=0), all but the n=1 term vanish and

$$v_{\perp 1} \equiv \frac{2\,\Omega_w\,\bar{v}_{\|}}{k_w r_b(k_w \bar{v}_{\|} - \bar{\Omega}_{\|})} I_1(k_w r_b)\, I_0(k_w r_g). \qquad (3)$$

Equation (3) reveals that the electron orbit can be controlled by adjusting B_0 and B_w. The solenoidal field B_0 not only provides the confinement of beam transport but also furnishes another knob to control $v_\perp$. The presence of the helical wiggler field in the interaction region tends to improve the confinement of the electron helical motion. As a consequence, high power electron beam may be utilized for the Peniotron interaction. For example, using V=225kV, B_0=15kG, B_w=2.2kG, and λ_w=1cm, the transverse electron spatial and velocity distributions just before entering the interaction region are shown in Fig. 1. The resulting $\alpha = v_\perp / v_{\|}$ is 0.6 in this case. In obtaining these results, a three spatial dimensional (realistic) wiggler field (Eq. 1) was used and an electron beam initially with only axial velocity was injected into a section of slowly varying amplitude wiggler field.

Using the parameters listed in table I, the relevent vaned waveguide modes (6 vanes) and harmonic wiggler beam lines are shown in Fig. 2a. There are three potential self-oscillating modes and their stabilities were investigated by carrying out single transverse mode simulations. Point A is the desired helical peniotron backward wave mode and is strongly unstable. Point B is the backward wave second harmonic free electron laser mode and is stable. Point C is the fundamental forward wave free elctron laser mode and is weakly unstable. The conventional cyclotron modes are not shown due to the smallness of $v_{\perp 0}$.

The time evolution of the wave power (TE_{31}) at z=0 and z=L from multi-mode simulations are shown i n Fig. 2b. The efficiency of the backward wave peniotron

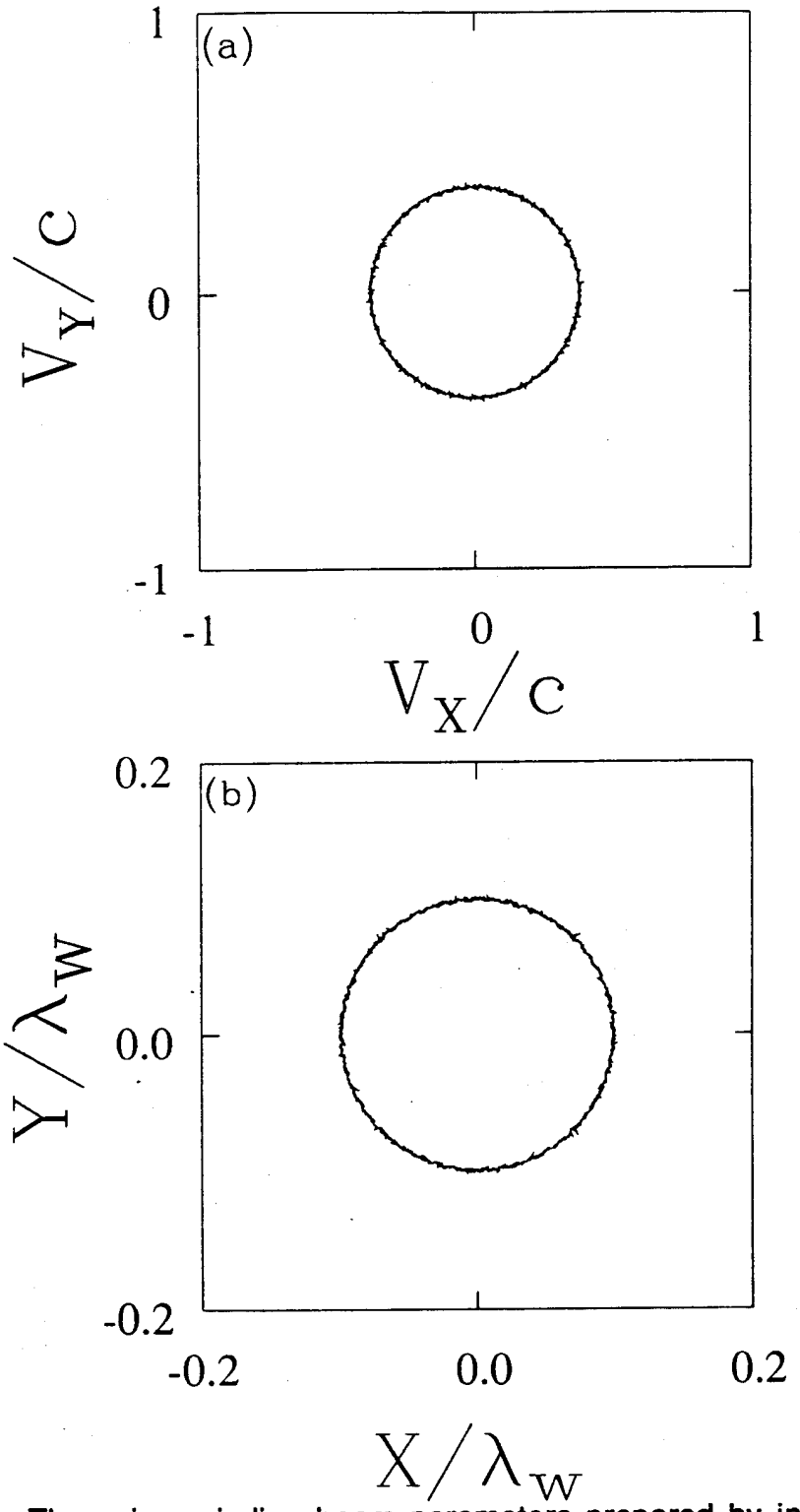

Figure 1 The axis-encircling beam parameters prepared by injecting an electron beam along the waveguide axis with $v_\perp=0$ into a combined solenoidal and wiggler field with slowly varyling wiggler amplitude, (a) v_y versus v_x and (b) y versus x.

TABLE I

Second Harmonic Helical Peniotron Backward Wave Oscillator

Beam Voltage	225 kV
Beam Current	50 A
Mode	π mode
Number of Vanes	6
$\alpha = v_\perp / v_\parallel$	0.6
Interaction Length (L)	10 cm
$\omega_c / 2\pi$	30.5 GHz
Inner Circuit Radius (a)	0.16 cm
Outer Circuit Radius (b)	0.304 cm
Guide Field (B_0)	15 kG
Wiggler Field (B_w)	2.2 kG
Wiggler Period (λ_w)	1 cm

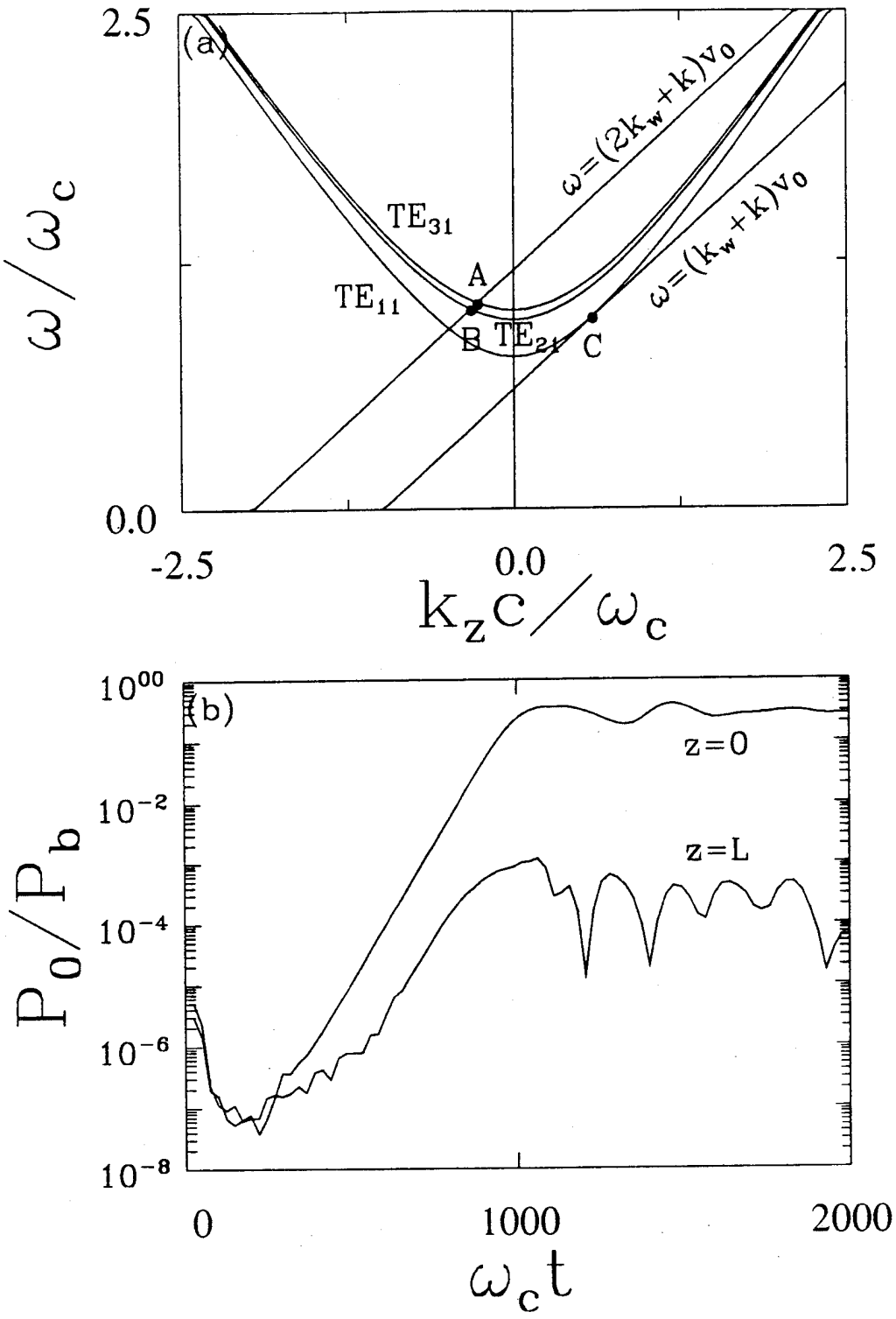

Figure 2 Self-oscillation in a combined solenoidal and wiggler field, (a) dispersion curves, and (b) time evolution of wave power (TE_{31}) at z=0 and L.

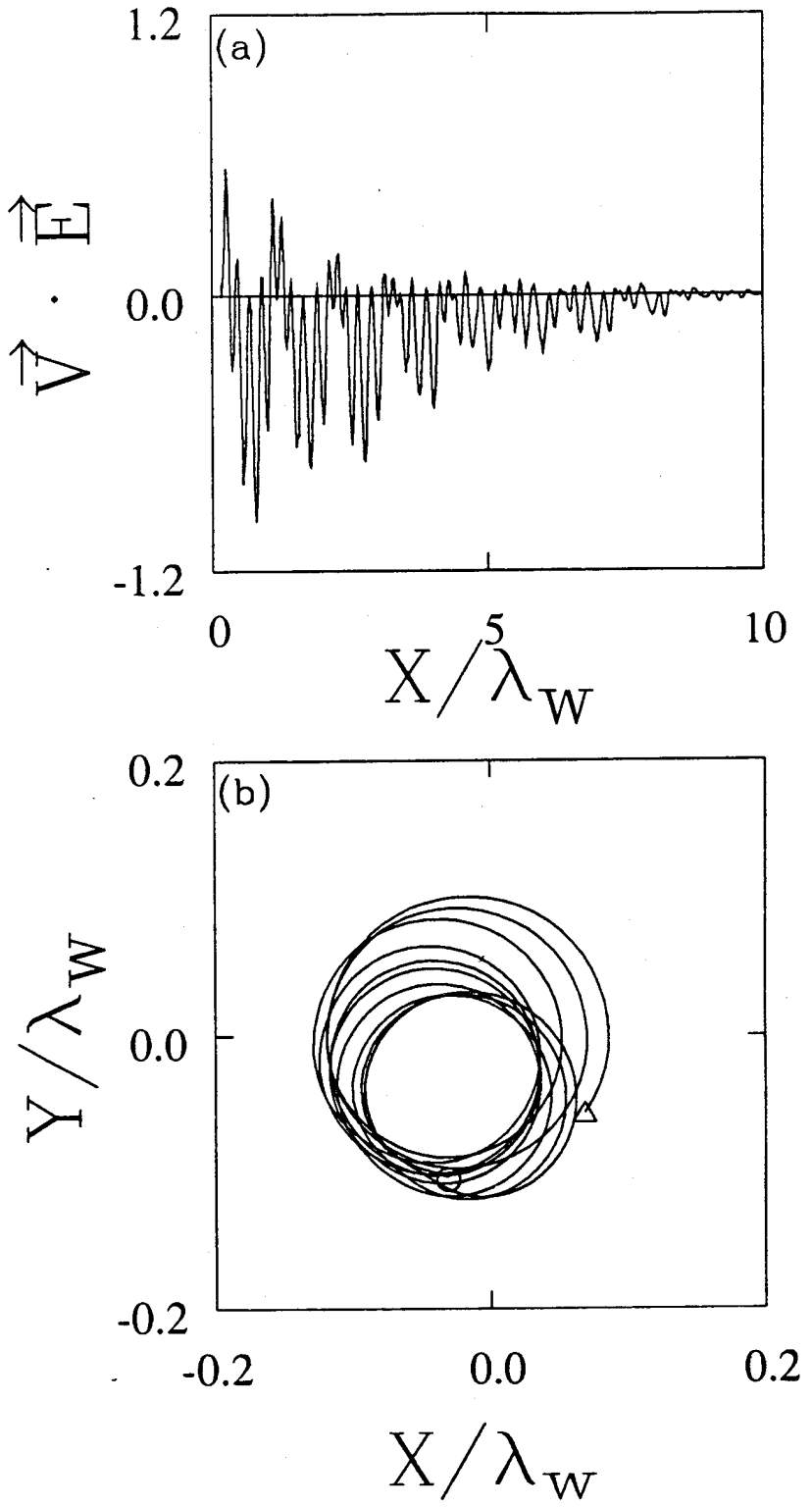

Figure 3 Test electron behavior when it travels through the interaction region, (a) electron-wave coupling and (b) its transverse trajectory.

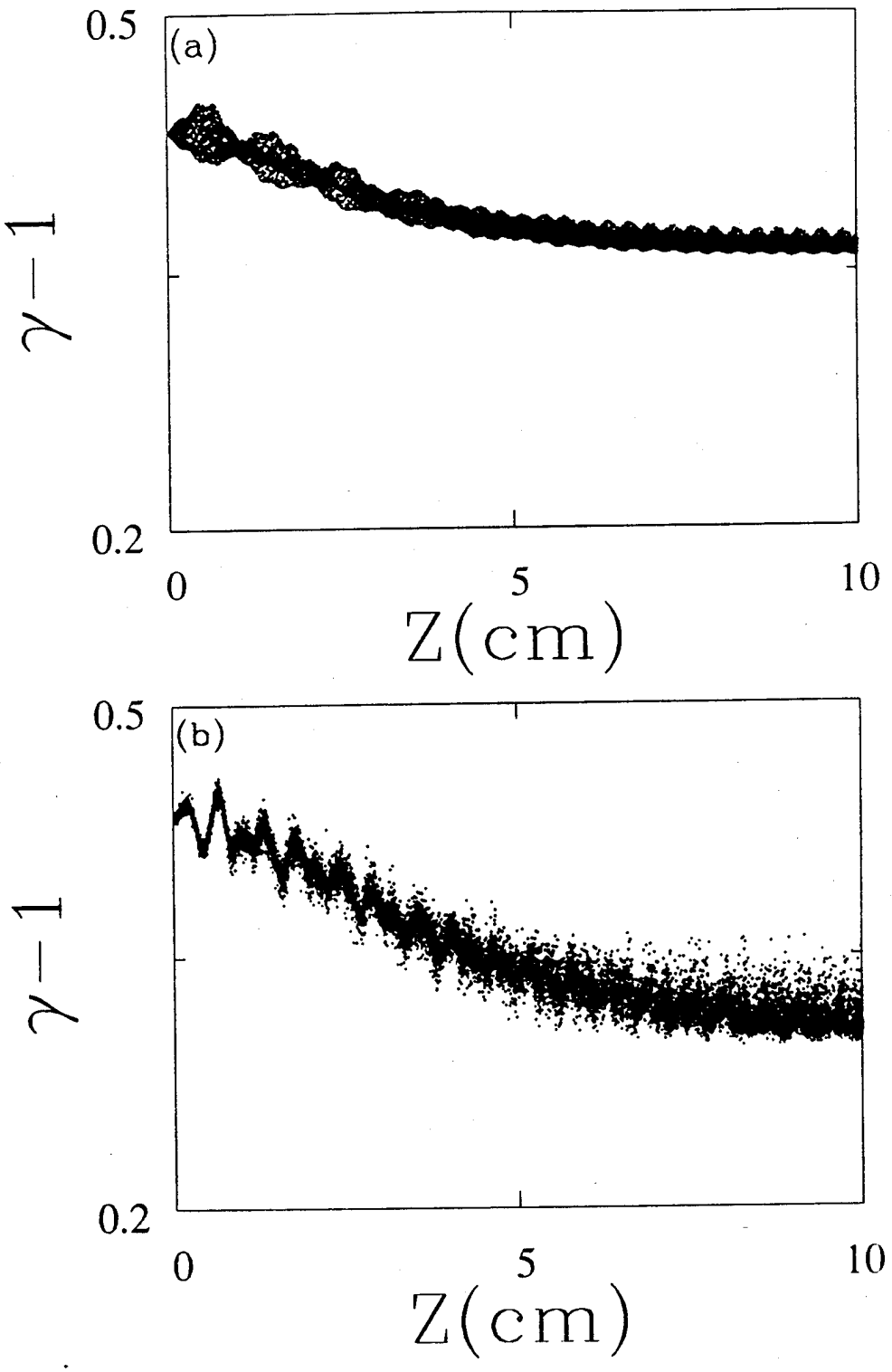

Figure 4 Electron energy versus axial distance at the time of saturation, (a) conventional peniotron interaction, (b) helical peniotron interaction.

interaction has attained about 30%. Figure 3 displays the test electron behavior when it travels through the interaction region. The electron-wave coupling result shows that on the average the test electron loses its energy to the wave while its transverse velocity plot illustrates its guiding center drift and the diminishing of its Larmor radius.

In order to make a comparison between the performance of a helical peniotron and conventional peniotron, simulations using the conventional axis-encircling beam with α=0.6 and Larmor radius equal to that of the helical beam were carried out. Figure 4 shows the electron energy versus the axial distance at the time of saturation for both cases. The result clearly demonstrates that after the beam-wave interaction all electrons lose energy to the wave which is the signature of the peniotron interaction. Furthermore it also indicates that the efficiency of a helical peniotron can attain twice that of a conventional peniotron. This significant difference in efficiency becomes even more clear when we show the time evolution of the electron kinetic energy after it interacts with the wave (Fig. 5) and is due to the fact that a conventional peniotron interaction tends to increase the beam longitudinal energy ($\gamma_{||}$)(Fig. 6a) because the phase velocity of its longitudinal ponderomotive force ($\vec{v}_{\perp} \times \vec{B}_{wave}$) is greater than C. On the other hand in a helical configuration the phase velocity of the ($\vec{v}_{w} \times \vec{B}_{wave}$) force is smaller than $v_{||}$ which results in decreasing $\gamma_{||}$ (Fig. 6a). Meanwhile, both interactions reduce the beam transverse energy (Fig. 6b). The resulting efficiency is 16% for the conventional Peniotron and 30% for the helical Peniotron.

The other potential advantage of a helical peniotron is that its gain mechanism does not rely on resonance interaction. Therefore its performance shall not be strongly affected by the velocity or guiding center spread. For example, using initial 3% axial velocity spread or 5% guiding center spread only reduce the efficiency by 2%.

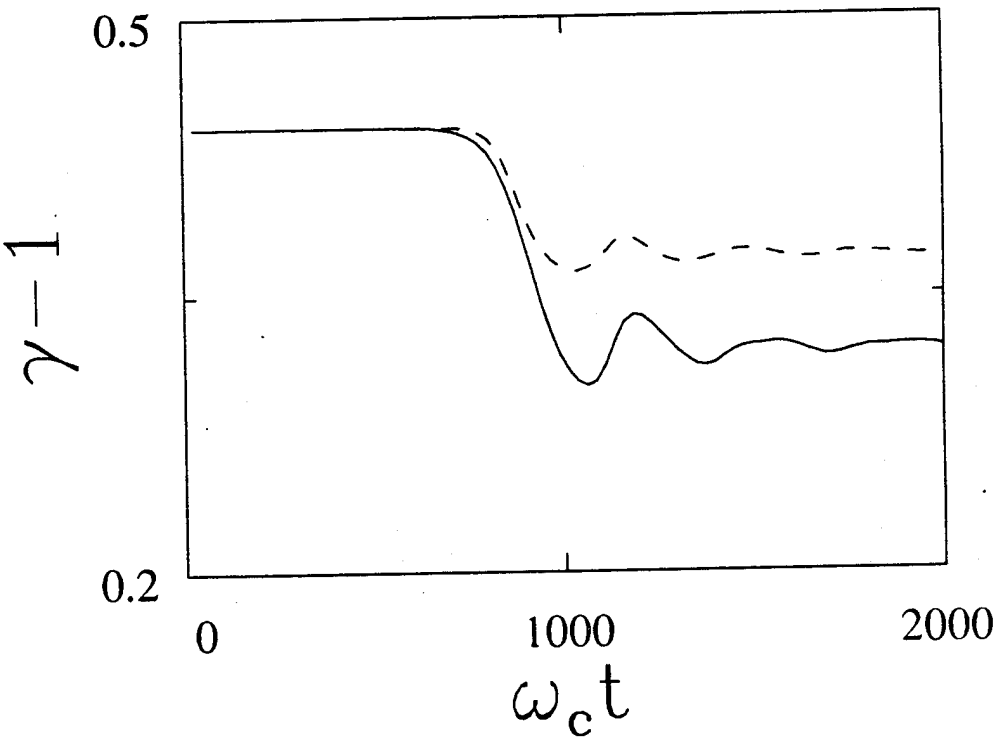

Figure 5 Time evolution of beam total energy at z=L, (solid line is for helical peniotron and dashed line is for conventional peniotron).

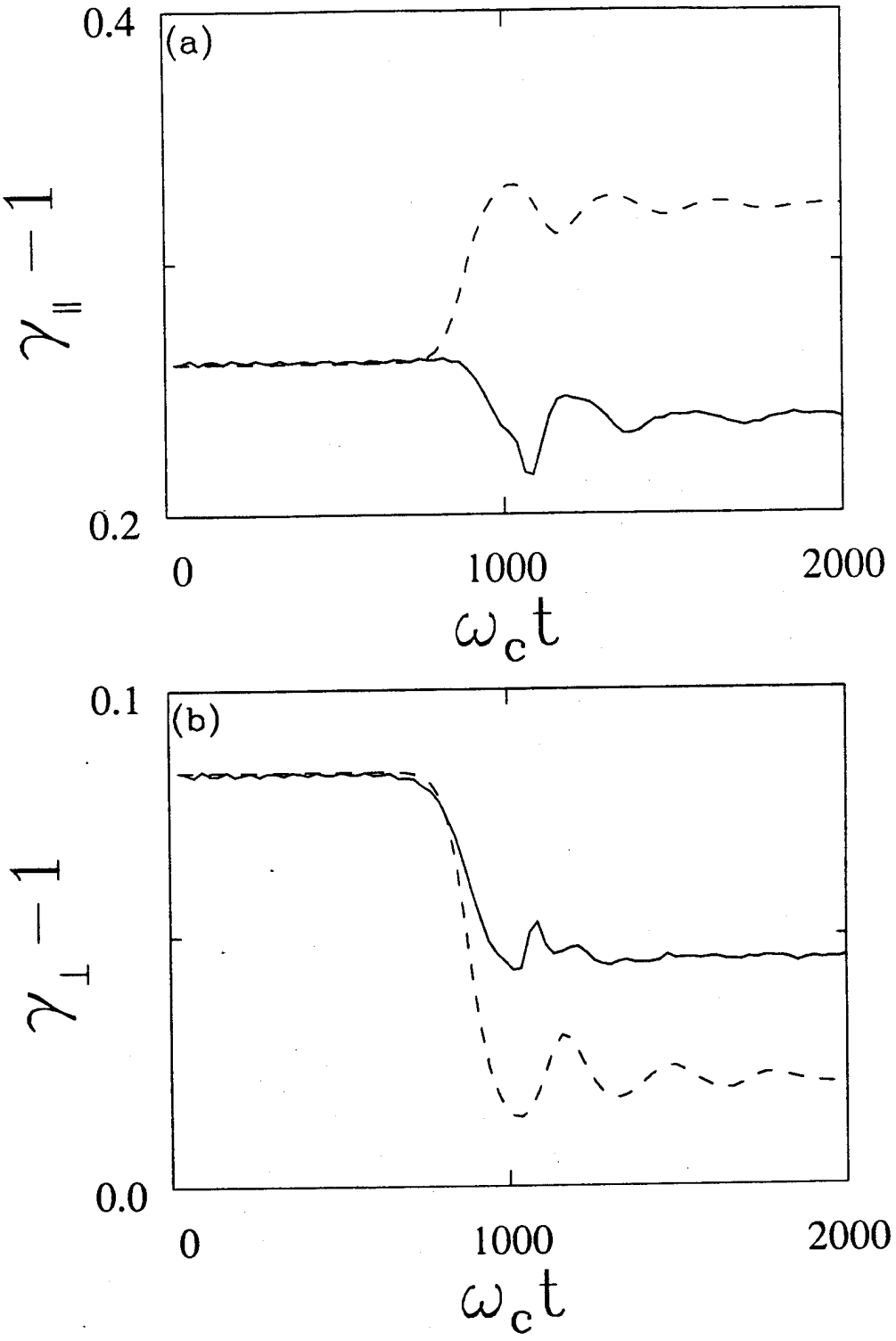

Figure 6 Time evolution of beam kinetic energy at z=L, (solid lines are for helical peniotron and dashed lines are for conventional peniotron). (a) beam longitudinal energy, and (b) beam transverse energy.

B. Peniotron Forward Wave Oscillations (Appendix I and II)

Even though the intrinsic feedback mechanism in an absolute instability is deleterious to an amplifier, it can be utilized to form an oscillator without a cavity structure. Backward wave oscillators which rely on a backward propagating electromagnetic wave to feedback the energy generated by the forward propagating beam have been built and performed rather well. As far as the absolute unstable mode which propagates in the positive k_z direction is concerned, experiments carried out so far were designed to avoid the excitation of this mode by using parameters below its starting oscillation condition. Meanwhile, theoreticians in plasma physics have suggested that the pulse spreading of the forward propagating absolute instability can be utilized to provide the feedback mechanism for establishing forward wave oscillations. This is equivalent to saying that if the temporal growth rate is faster than the energy convection rate at $z=z_0$, the forward propagating self-oscillation can be excited. We have carried out simulations to demonstrate the feasibility of building a peniotron forward oscillator. We also observed that the peniotron interaction is able to suppress the gyrotron interaction in all the cases simulated. The results indicate that the presence of the gyrotron interaction even when it reaches large amplitude may affect only the temporal growth rate of the peniotron interaction, which requires no phase bunching but not its final efficiency. This is because a saturated gyrotron mode (resonance interaction) induces only effective beam guiding center (changing electron Larmor radius) and velocity spreads but no guiding center drift to a peniotron interaction which would reduce only the temporal growth rate. An experiment at UC Davis has also been built to test the novel idea we have proposed (Appendix III).

C. Pulsating Mode in Peniotron Backward Wave Oscillations (Appendix IV)

Increasing the current or interaction length in self-oscillating interactions tends to change the output wave from a smooth oscillation to a relaxation oscillation and

eventually to become choatic. However, in carrying out computer simulations to investigate the performance of peniotron backward wave oscillators, we observed that due to its unique electron-wave energy exchange process, a sustainable self-pulsing mode can be excited if parameters are properly chosen. This new mode of operation can only be established if, at some instant of time the reduction in beam energy resulting from the electron-wave interaction is to such an extent that its cyclotron harmonic line itersects with the vaned waveguide dispersion cureve in the positive k_z region. The generation of the forward traveling self-oscillating mode eliminates the residual backward traveling wave, which is very essential in establishing a relaxation oscillation. As a result, the time evolution of the output wave becomes self-pulsating. The pulsating frequency is approximately equal to the difference between the initial and the later time cyclotron lines when the output wave is at its peak.

III. AFOSR Supported Publications (October 1, 1993--September 30, 1994)

1. A.T. Lin and Chih-Chien Lin, "Peniotron forward wave self-oscillations," Appl. Phys. Lett. 64, 1088(1994).

2. A. T. Lin, C. K. Chong, D. B. McDermott, A. J. Balkcum, F. V. Hartmann, and N. C. Luchmann, Jr., "Slotted third-harmonic peniotron forward-wave oscillator," Proceeding of 1994 S.P.I.E. Conf. on Intense Microwave Pulses(1994).

3. A.T. Lin and Chih-Chien Lin, "Pulsating mode in peniotron backward wave oscillations," Phys. of Plasma, 1, December (1994).

4. A.T. Lin and Chih-Chien Lin, "Gyro peniotron forward wave oscillators," IEEE Trans. on Plasma Science 22, October(1994).

APPENDICES

1. Peniotron forward wave self-oscillators.

2. Gyro peniotron forward wave oscillators.

3. Slotted third-harmonic peniotron forward-wave oscillators.

4. Pulsating mode in peniotron backward wave oscillations.

APPENDIX 1

Peniotron forward wave self-oscillations

A. T. Lin and Chih-Chien Lin
Department of Physics, University of California at Los Angeles, Los Angeles, California 90024-1547

(Received 16 November 1993; accepted for publication 20 December 1993)

The forward propagating absolute instability in peniotron interaction can be utilized to build forward wave oscillators. This is demonstrated by performing computer simulations which also reveal that the peniotron interaction is able to suppress the gyrotron interaction and attains the efficiency without the influence of the gyrotron mode.

Microwave source derived from peniotron mechanism was conceived almost three decades ago.[1] Since then many investigators have carried out theoretical calculations[2,3] and attempted to employ various beam and electrodynamic configurations[4] to illustrate the aspect of high efficiency peniotron harmonic interaction. Up to now there is still no convincing evidence to assure that high efficiency interaction has been achieved in any of the experiments. However, from past experience a consensus has been reached that the essential elements for efficient peniotron operation are a electrodynamic configuration which is capable of providing a positive radial gradient in the microwave field distribution and an axis-encircling beam which initially can be placed at a high beam-wave coupling position. Recently, based on these important informations, the parameters of a peniotron amplifier[5] were proposed and a high quality factor ($Q \simeq 2000$) peniotron oscillator was built.[4] The former has to avoid various self-oscillation which could degrade or totally prohibit the amplification process. This constraint forces one to contemplate a multisection device with the length of each section below the starting oscillations length of all the potential oscillations. The high quality factor of the latter tends to require a well matched external load to couple out the major portion of the stored energy. It is also suspected that the experimental peniotron output[4] may be contaminated by the nearby gyrotron oscillation. In this letter we propose an alternative peniotron oscillator configuration without providing external reflection which alleviates the difficulty of finding a well matched load circuit. This is based on the self-oscillation of the forward propagating absolute instability which can be chosen to be the dominant interaction in the system. In investigating the peniotron and gyrotron competition, simulation results reveal that the peniotron interaction always suppresses the gyrotron interaction if the beam guiding center spread is moderate (<30%). This understanding should be helpful in interpreting the experimental result of conventional peniotron oscillators.[4] Simulation results are also capable of determining the starting oscillation length of absolute instability which is an important information for building a peniotron amplifier.

Because of its boundary conditions, the harmonic field in an azimuthally corrugated interaction structure which was originally introduced for high harmonic gyrotron operations[6] becomes stronger when it gets closer to the waveguide wall and is therefore also suitable for the peniotron interaction. In the interaction region, the electric and magnetic fields of a transverse electric field mode[7] may be written as $E_n = E_{Tn}(z,t)(\hat{z}\times\nabla_\perp C_n)$ and $B_n = B_{Tn}(z,t)\nabla_\perp C_n + \hat{z}B_{Ln}k_\perp C_n$, where C_n is the local wave function and can be expressed as

$$C_n = -\sum_{m=-\infty}^{\infty} \frac{A_\Gamma}{k_\perp} J_\Gamma(k_\perp r)e^{j\Gamma\theta}.$$

Here $\Gamma = n + mN, n = 0,1,\ldots,N/2$, m is any integer, N is the number of vanes, and $A_\Gamma = (N\theta_0/\pi)(\sin\Gamma\theta_0/\Gamma\theta_0)$ is the enhancement factor of the slotted structure. $k_\perp$ is the cutoff wave number which can be determined from the circuit dispersion relation

$$\sum_\Gamma \frac{J_\Gamma(k_\perp a)}{J'_\Gamma(k_\perp a)}\left(\frac{\sin\Gamma\theta_0}{\Gamma\theta_0}\right)^2 = -\frac{\pi}{N\theta_0}\frac{Z_0(k_\perp a)}{Z_1(k_\perp a)}, \tag{1}$$

where Z_Γ is a combination of Bessel function (J_Γ) and Neumann function (N_Γ) of order Γ, $Z_\Gamma(x) = J_\Gamma(x) - J_1(k_\perp b)/[N_1(k_\perp b)]N_\Gamma(x)$ and $\theta_0 = 2\pi/4N$. Here a and b denote, respectively, the inner and outer circuit radius. For each value of n, there are infinite number of solutions from Eq. (1). The first root is the most important one and the associated mode is usually designated by TE_{n1}. The mode number n is also the number of times the rf field pattern repeats in one rotation around the waveguide axis. There are many possible modes but the two most interesting cases are the π mode where adjacent slots are out of phase by π, and the 2π mode where the phase in each slot is identical. In the most rigorous description an infinite superposition of different Γ's is required to represent each n mode. However in most of the cases an adequate approximation includes just two partical waves—those with $\Gamma = n$ and $(n-N)$. The physical meaning of this is that an electromagnetic wave rotating in a periodic structure must interfere with other waves to reproduce the static periodic pattern of the structure. The outgoing wave boundary conditions are imposed in simulations.

The modes supported by the slotted structure can interact with an axis-encircling electron beam through the relativistic gyrotron and nonrelativistic peniotron mechanisms. In a gyrotron interaction[8] ($n = s$, s is the harmonic number), an initially randomly phased electron beam would end up with some of its electrons giving up energy to and the rest of them absorbing energy from the same wave. On the other hand the gain mechanism underlines a peniotron interaction ($n = s + 1$) is due to the electron guiding center drift in a nonuniform rf field so that during a cyclotron orbit an electron on the average is in a stronger rf field region during the decel-

 0003-6951/94/64(9)/1088/3/$6.00

TABLE I. Second harmonic vaned peniotron oscillator design.

Beam voltage	70 kV
Beam current	3.5 A
Magnetic field	6.5 kG
Mode	π mode
Number of vanes	6
$\alpha=v_\perp/v_\parallel$	1.2
B_0/B_g	1
$\omega_c/2\pi$	33.65 GHz
Inner circuit radius (a)	0.16 cm
Outer circuit radius (b)	0.304 cm

erating phase and in a weaker rf field region during the accelerating phase. As a result all electrons regardless of their initial phases relative to the wave convert their kinetic energy into wave energy and makes peniotron devices inherently high efficiency.

An unavoidable feature of a vaned waveguide is the small frequency separation between the modes of larger n which renders the mode competition in peniotron device an important issue to be addressed. Using the parameters of Table I, the dispersion curves of the relevant waveguide modes are shown in Fig. 1(a). The first three cyclotron harmonic ($s=1,2,3$) lines are also plotted in the same figure. There are three potential oscillation sources which are marked by points 1, 2, and 3. They all have their own starting oscillation lengths. Points 2 and 3 are the conventional gyrotron backward wave modes with relatively low efficiency. Point 1 is the desired peniotron mode which is capable of producing high efficiency output as well as large temporal growth rate due to its grazing interaction.

The intrinsic feedback mechanism in an absolute instability even though it is deleterious to an amplifier can be

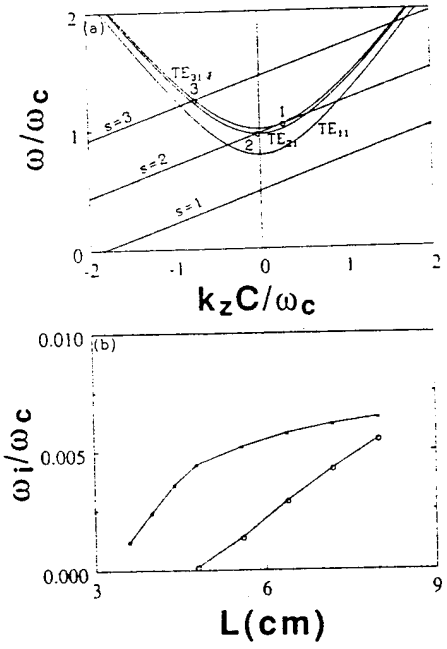

FIG. 1. Six vane slotted waveguide and an axis encircling beam: (a) Dispersion curves, (b) temporal growth rate vs system length (star: TE_{31}, circle: TE_{21}).

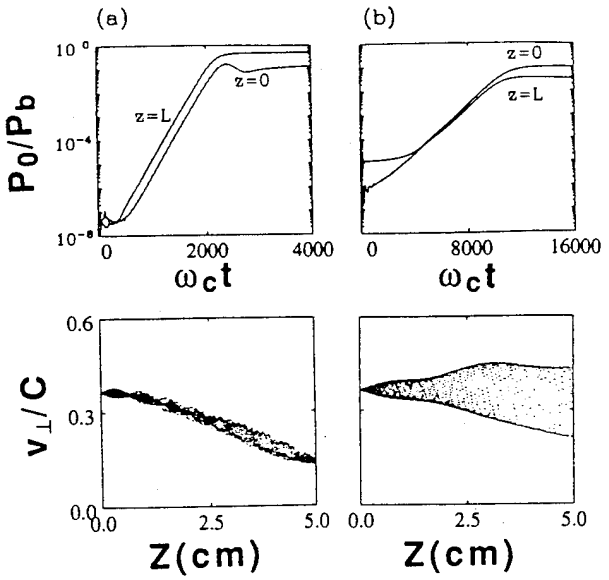

FIG. 2. Time evolution of wave power (P_0) normalized to beam power (P_b) for $L=5$ cm and electron perpendicular velocity vs axial distance (a) peniotron interaction (TE_{31}) and (b) gyrotron interaction (TE_{21}).

utilized to form an oscillator without a cavity structure. The theoretical investigations of the absolute instability for either gyrotrons[8] or peniotrons[9] are all based on the pinch-point theory which was first derived in plasma physics for an infinite homogeneous medium. However, an absolute instability in a limited spatial extent may be stable. In order to illustrate the effects of system length on the competition among various absolute unstable modes, we have first carried out single transverse mode computer simulations to evaluate their temporal growth rate vs interaction length and results are shown in Fig. 1(b). The starting oscillation length can be determined by extending the growth rate curve to intersect the length axis. The time evolution of the wave power (TE_{31} mode) from the peniotron interaction at $z=0$ and L for the $L=5$ cm case is plotted in Fig. 2(a). The results clearly illustrate that initial perturbations grow in time at every point in the interaction space with the same growth rate which is the signature of an absolute instability. The direction of power flow determined by performing local Poynting flux calculation $\mathbf{E}_T\,\mathbf{B}_T$ is along the beam propagating direction and the output power attained more than 50% of the beam input power. In the range of $L\leq 10$ cm, there is no trace of exciting the backward wave of point 3 [Fig. 1(a)]. Using the same system length and retaining only the TE_{21} mode, the time evolution of the wave power at both ends is shown in Fig. 2(b). In this case the instability arises from the gyrotron backward wave interaction. The efficiency has reached only about 10% and the wave power flow is in the backward direction. Notice that the wave amplitude at $z=L$ is not negligible in comparison with that of at $z=0$ because point 2 [Fig. 1(a)] is so close to the waveguide cutoff. In order to demonstrate the difference between the peniotron and the gyrotron interactions, their respective electron perpendicular velocity in the entire interaction space at $\omega_c t=6000$ is displayed in Fig. 2. Simulation results clearly reveal that as a result of the peniotron interaction all electrons irrespective of their initial

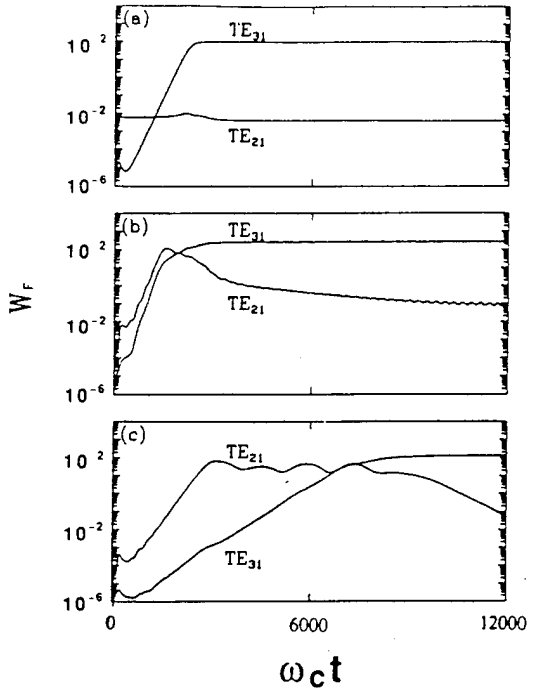

FIG. 3. Time evolution of stored wave energy from multimode simulations. (a) $L=5$ cm, $I=3.5$ A, (b) $L=8$ cm, $I=3.5$ A, and (c) $L=8$ cm, $I=1.5$ A.

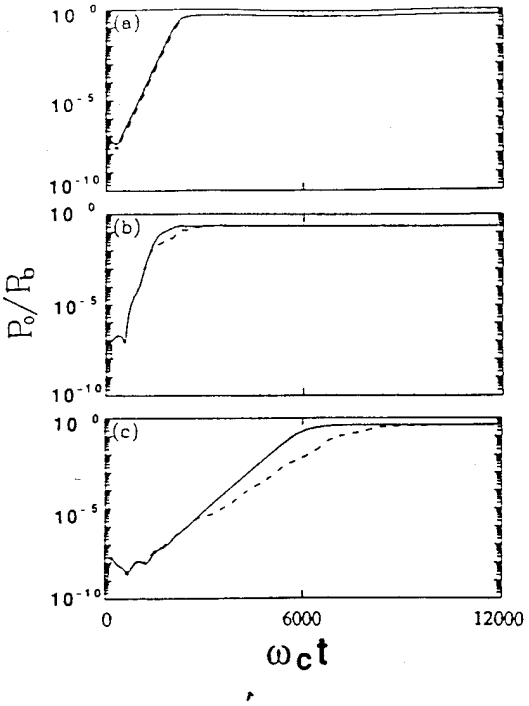

FIG. 4. Time evolution of peniotron output wave power (solid curve is from single mode simulation, dashed curve is from multi mode simulation): (a) $L=5$ cm, $I=3.5$ A, (b) $L=8$ cm, $I=3.5$ A, and (c) $L=8$ cm, $I=1.5$ A.

phase give up their energies to the wave while the gyrotron interaction results in that only part of electron beam loses energy and the remaining part gains energy.

As is known, an absolute instability grows from the initial fluctuation of the system eigenmodes and is eventually saturated by some nonlinear mechanism. Therefore, by properly choosing the parameters one should be able to turn it into a useful microwave source. Based on our preliminary simulation results which will be presented later, the proposed mechanism possesses certain unique characteristics which make it a very attractive and viable peniotron microwave source.

To assure that the oscillation from the TE_{21} mode would not deteriorate the performance of the desired peniotron operation, multimode simulations were carried out. Figure 3 shows the time evolution of the stored energy in the interaction space for three different cases. With $L=5$ cm [Fig. 3(a)] the initial growth of the TE_{21} mode comes from the convective unstable mode with positive k_z and the growth rate of its absolute unstable mode is so small that it can be easily suppressed by the growth of the TE_{31} mode. Lengthening the system length to 8 cm tends to enhance the gyrotron interaction more than to the peniotron interaction. In this case the two interactions have about the same growth rate [Fig. 3(b)]. The peniotron mode eventually is able to suppress the gyrotron mode. Using $L=8$ cm and $I=1.5$ A [Fig. 3(c)] the temporal growth rate of the gyrotron interaction now surpasses that of the peniotron interaction. However, the peniotron interaction is still able to suppress the gyrotron interaction. The respective time evolution of the peniotron output power of the three cases described in Fig. 3 is shown in Fig. 4. Both single mode and two mode simulations are presented. The results indicate that the presence of the gyrotron interaction when it reaches large amplitude may affect the temporal growth rate of the peniotron interaction which requires no phase bunching but not its final efficiency for all three cases. This is because that to a peniotron interaction a saturated gyrotron mode induces an effective beam guiding center and perpendicular velocity spreads which would reduce the temporal growth rate. Since at the end the gyrotron mode is completely suppressed and returns to its noise level, the peniotron mode should be able to attain the efficiency without the influence of the gyrotron mode.

This work was supported by the Air Force Office of Scientific Research under Grant No. AFOSR 91-0006 and the San Diego Supercomputing Center.

[1] K. Yamanouchi, S. Ono, and Y. Shibata, *Proceedings of the 5th International Microwave Tube Conference, Paris* (Academic, London, 1964), p. 321.
[2] A. K. Ganguly, S. Ahn, and S. Y. Park, Int. J. Electron. **65**, 597 (1988).
[3] P. S. Rha, L. R. Barnett, J. M. Baird, and R. W. Grow, IEEE Trans. Electron Devices **36**, 789 (1989).
[4] K. Yokoo, H. Shimawaki, H. Tadano, T. Ishihara, K. Sagae, N. Sato, and S. Ono, *17th International Conference on Infrared and Millimeter Waves* (SPIE, Bellingham, WA, 1992), p. 498.
[5] G. S. Park, J. L. Hirshfield, R. H. Kyser, C. M. Armstrong, and A. K. Gauguly, *17th International Conference on Infrared and Millimeter Waves* (SPIE, Bellingham, WA 1992).
[6] Y. Y. Lau and L. R. Barnett, Int. J. Infrared Millimeter Waves **3**, 619 (1982).
[7] T. H. Kho and A. T. Lin, Nucl. Instrum. Methods Phys. Res. A **296**, 642 (1990).
[8] K. R. Chu and A. T. Lin, IEEE Trans. Plasma Sci. **16**, 90 (1988).
[9] A. K. Ganguly, Y. Y. Lau, and S. Ahn, Phys. Fluids B **4**, 3800 (1992).

APPENDIX 2

Gyro Peniotron Forward Wave Oscillators

A. T. Lin and Chih-Chien Lin

Abstract— The pulse spreading of the forward propagating absolute instability in gyro-peniotron interaction can be utilized to provide the feedback mechanism for establishing forward wave oscillators. By properly choosing the interaction length and beam current, high efficiency stable output at high harmonic operation can be attained. This is demonstrated by performing computer simulations which also reveal that the peniotron interaction is able to suppress the gyrotron interaction and reaches the maximum efficiency despite the influence of the gyrotron mode.

I. Introduction

A microwave source derived from the peniotron mechanism was conceived almost three decades ago [1]. Since then many investigators have carried out theoretical calculations [2]-[5] and attempted to employ various beam and electrodynamic configurations [6], [7] to illustrate the aspect of high efficiency peniotron harmonic interaction. Up to now there is still no convincing evidence to assure that high efficiency interaction has been achieved in any of the experiments. However from past experience a consensus has been reached that the essential elements for efficient peniotron operation are an electrodynamic configuration which is capable of providing a positive radial gradient in the microwave field distribution and an axis-encircling beam which initially can be placed at a high beam-wave coupling position. Recently, based on this important information, the parameters of a peniotron amplifier [8] were proposed and a high quality factor ($Q \simeq 2000$) peniotron oscillator was built [7]. The former has to avoid various self oscillations which could degrade or totally prohibit the amplification process. This constraint forces one to contemplate a multi-section device with the length of each section below the starting oscillation length of all the potential oscillations. The high quality factor of the latter tends to require a well matched external load to couple out the major portion of the stored energy. It is also suspected that the experimental peniotron output [7] may be contaminated by the nearby gyrotron oscillation. In this paper we propose an alternative peniotron oscillator configuration without external reflection which alleviates the difficulty of finding a well matched load circuit. The feedback mechanism is provided by the pulse spreading of the forward propagating absolute instability which can be chosen to be the dominant interaction in the system. The proposed configuration may be considered as the first step to demonstrate that the peniotron interaction is capable of attaining high efficiency. In investigating the peniotron and gyrotron competition, simulation results reveal that the peniotron interaction always suppresses the gyrotron interaction if the beam guiding center spread is moderate ($< 30\%$). This understanding should be helpful in interpretating the experimental result of conventional peniotron oscillators [7]. Simulation results are also capable of determining the starting oscillation length of absolute instability which is important information for a peniotron amplifier.

Manuscript received August 31, 1993; revised June 24, 1994. This work was supported by the Air Force Office Of Scientific Research under Grant No. F49620-93-1-0628 and the San Diego Supercomputing Center.

The authors are with the Department of Physics, University of California at Los Angeles, Los Angeles, CA 90024-1547 USA.

IEEE Log Number 9404578D.

II. Numerical Model

Because of its boundary conditions, the harmonic field in an azimuthally corrugated interaction structure originally introduced for high harmonic gyrotron operation [9], [10] becomes stronger when it gets closer to the waveguide wall and is therefore also suitable for the peniotron interaction. The cross-sectional view of a six vane slotted waveguide with an axis-encircling beam is displayed in Fig. 1(a). In the interaction region, the electric and magnetic fields of a transverse electric field model [11], [12] may be written as

$$E_n = E_{Tn}(z,t)(\hat{z} \times \nabla_\perp C_n) \tag{1}$$

$$B_n = B_{Tn}(z,t)\nabla_\perp C_n + \hat{z} B_{Ln} k_\perp C_n, \tag{2}$$

where C_n is the local wave function

$$C_n = -\sum_{m=-\infty}^{\infty} \frac{A_\Gamma}{k_\perp} J_\Gamma(k_\perp r) e^{j\Gamma\theta}. \tag{3}$$

Here $\Gamma = n + mN, n = 0, 1, ..., N-1; m$ is any integer, N is the number of vanes, and $A_\Gamma = \frac{N\theta_0}{\pi} \cdot \frac{\sin\Gamma\theta_0}{\Gamma\theta_0}$ is the enhancement factor of the slotted structure. $k_\perp$ is the cutoff wavenumber which can be determined from the circuit dispersion relation

$$\sum_\Gamma \frac{J_\Gamma(k_\perp a)}{J'_\Gamma(k_\perp a)} \left(\frac{\sin\Gamma\theta_0}{\Gamma\theta_0}\right)^2 = -\frac{\pi}{N\theta_0} \frac{Z_0(k_\perp a)}{Z_1(k_\perp a)}, \tag{4}$$

where Z_Γ is a combination of Bessel function (J_Γ) and Neumann function (N_Γ) of order Γ

$$Z_\Gamma(x) = J_\Gamma(x) - \frac{J_1(k_\perp b)}{N_1(k_\perp b)} N_\Gamma(x), \tag{5}$$

and $\theta_0 = 2\pi/4N$. Here a and b denote respectively the inner and outer circuit radius. For each value of n, there are an infinite number of solutions from (4). The first root is the most important one and the associated mode is usually designated by TE_{n1}. The mode number n is also the number of times the RF field pattern repeats in one rotation around the waveguide axis. There are many possible modes but the two most interesting cases are the π mode, where adjacent slots are out of phase by π, and the 2π mode, where the phase in each slot is identical.

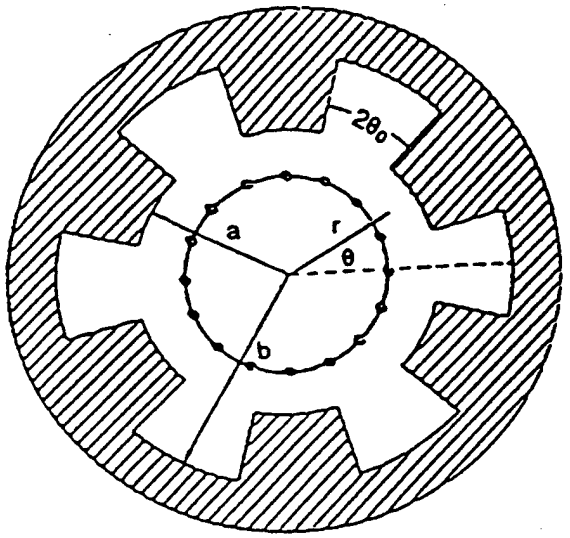

(a)

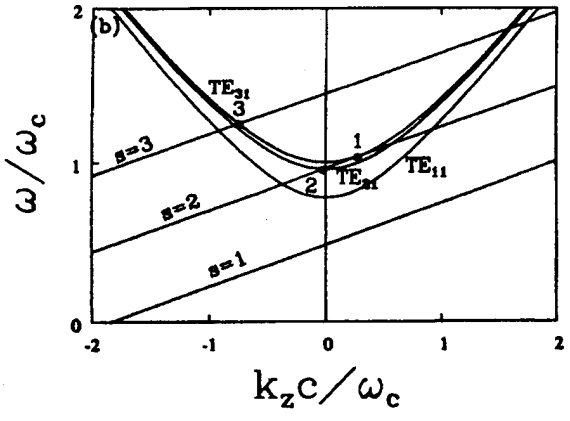

(b)

Fig. 1. Six vane slotted waveguide and an axis encircling beam: (a) cross-sectional view (the dots are schematic repreesentation of beam electrons) and (b) dispersion curves.

In the most rigorous description an infinite superposition of different Γ's is required to represent each n mode. However in most of the cases an adequate approximation includes just two partial waves—those with $\Gamma = n$ and $(n - N)$. The physical meaning of this is that an electromagnetic wave rotating in a periodic structure must interfere with other waves to reproduce the static periodic pattern of the structure.

The modes supported by the slotted structure can interact with an axis-encircling electron beam through the relativistic gyrotron and non-relativistic peniotron mechanisms. In a gyrotron interaction it is necessary that an electron stays approximately in the same phase with respect to the wave as it traverses through the interaction region so that the cumulative electron-wave interaction produces a substantial bunching through the relativistic mass effect. As a consequence, an initially randomly phased electron beam would end up with some of its electrons giving up energy to and the rest of them absorbing energy from the same wave. This resonant condition

TABLE I
SECOND HARMONIC VANED PENIOTRON OSCILLATOR DESIGN

Beam Voltage	70 kV
Beam Current	3.5 A
Magnetic Field	6.5 kG
Mode	π mode
Number of Vanes	6
$\alpha = v_\perp / v_\parallel$	1.2
B_0/B_g	1
$\omega_c/2\pi$	33.65 GHz
Inner Circuit Radius (a)	0.16 cm
Outer Circuit Radius (b)	0.304 cm

can be expressed as

$$\omega_0 = k_z v_z + s\frac{\Omega_c}{\gamma}, \tag{6}$$

where ω_0 and k_z are respectively the wave frequency and axial wavenumber. v_z and γ are the electron axial velocity and relativistic factor. Ω_c is the non-relativistic cyclotron frequency and s is the harmonic number. For efficient gyrotron interaction n must be equal to s. On the other hand, the gain mechanism underlying a peniotron interaction is due to the electron guiding center drift so that during a cyclotron orbit an electron on the average is in a stronger RF field region during the decelerating phase and in a weaker RF field region during the accelerating phase. This is due to the fact that an accelerated electron increases its radius of gyration and the requirement $n = s+1$ which ensures that in our example (Fig. 1(a)) half of the cyclotron orbit is accelerating while the other half is decelerating. As a result all electrons, regardless of their initial phases relative to the wave, convert their kinetic energy into wave energy. This makes peniotron devices inherently high-efficiency.

An unavoidable feature of a vaned waveguide is the small frequency separation between the modes of larger n, which renders the mode competition in peniotron devices an important issue to be addressed. Using the parameters of Table I, the dispersion curves of the relevent waveguide modes are shown in Fig. 1(b). Here, $\omega_c = \frac{k_\perp c}{a}$, c is the speed of light, B_0 is the applied external magnetic field, and B_g is the magnetic field for grazing interaction. The first three cyclotron harmonic ($s = 1, 2, 3$) lines are also plotted in the same figure. There are three potential oscillation sources which are marked by points 1, 2 and 3. They all have their own starting oscillation lengths. Points 2 and 3 are the conventional gyrotron backward wave modes with relatively low efficiency. Point 1 is the desired peniotron mode which is capable of producing high efficiency output as well as large temporal growth rate due to its grazing interaction.

III. SIMULATION RESULTS

Even though the intrinsic feedback mechanism in an absolute instability is deleterious to an amplifier, it can be utilized to form an oscillator without a cavity structure. Gyrotron backward wave oscillators [13], [14] which rely on a backward propagating electromagnetic wave to feedback the energy generated by the forward propagating beam have been built

and performed rather well. As far as the absolute unstable mode at point 1 (Fig. 1(b)) is concerned, experiments carried out so far were designed to avoid the excitation of this mode by using parameters below its starting oscillation condition.

The theoretical investigations of the absolute instability for either gyrotrons [15], [16] or peniotrons [17] are all based on the pinch-point theory which was first derived in plasma physics for an infinite homogeneous medium [18]. However, an absolute instability in a limited spatial extent may be stable. In order to illustrate the effects of system length on the competition among various absolute unstable modes, we have first carried out single transverse mode computer simulations to evaluate their temporal growth rate versus interaction length. The results are shown in Fig. 2(a). In the simulations, the electrons are continuously injected at $z = 0$ with prescribed parameters and collected at $z = L$. Initially, the axial-encircling electrons fill up the interaction region uniformly along the z-direction. Resistive layers are provided on both sides of interaction region to absorb the outgoing electromagnetic waves. The starting oscillation length can be determined by extending the growth rate curve to intersect the z axis. The time evolution of the wave power (TE_{31} mode) from the peniotron interaction at $z = 0$ and L for the $L = 5$ cm case is plotted in Fig. 2(b). The results clearly illustrate that initial perturbations grow in time at every point in the interaction space with the same growth rate which is the signature of an absolute instability. The direction of power flow determined by performing local Poynting flux calculation $\vec{E}_T \times \vec{B}_T$ is along the beam propagating direction and the output power attained more than 50 % of the beam input power. It was also observed in simulations that a broad spectrum of k's was excited and they all propagate in the forward direction. In the range of $L \leq 10$ cm, there is no trace of exciting the backward wave of point 3 (Fig. 1(b)). Using the same system length and retaining only the TE_{21} mode, the time evolution of the wave power at both ends is shown in Fig. 2(c). In this case the instability arises from the gyrotron backward wave interaction. The efficiency has reached only about 10 % and the wave power flow is in the backward direction. Notice that the wave amplitude at $z = L$ is not negligible in comparison with that at $z = 0$ because point 2 (Fig. 1(b)) is so close to the waveguide cutoff. In order to demonstrate the difference between the peniotron and the gyrotron interactions, the electron perpendicular velocity in the entire interaction space at $\omega_c t = 6000$ is displayed in Fig. 3. Simulation results clearly reveal that as a result of the peniotron interaction all electrons irrespective of their initial phase, give up their energies to the wave, while in the gyrotron interaction only part of electron beam loses energy and the remaining part gains energy.

An unstable system will, in general, have a range of k_z values with positive $\omega_i(k_z)$ and an initial disturbance will excite a spectrum of k_z's. In a weakly unstable system with beam current below the threshold for oscillation, the instability is convective. The disturbance like point 1 in Fig. 1(b) propagates in the forward direction and the pulse will spread to each side of the peak. As the beam current is increased to such an extent that the growth rate is strong enough to cause the signal to grow at the very point of the initial disturbance by pulse spreading, the instability becomes absolute.

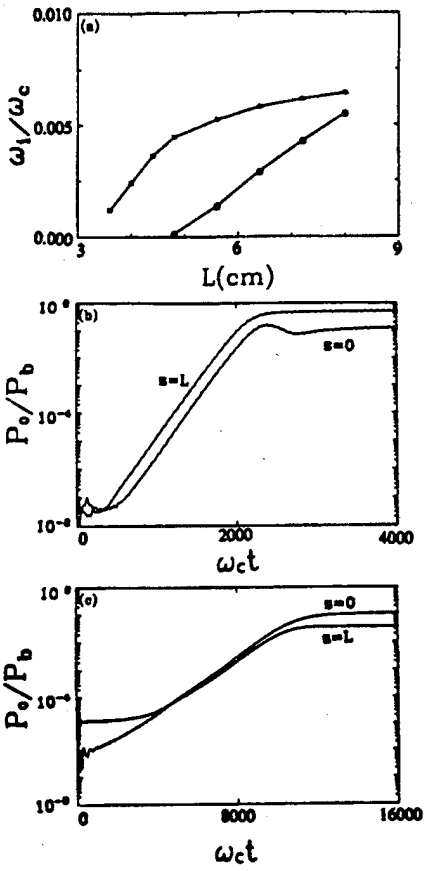

Fig. 2. Self oscillations in finite length system: (a) temporal growth rate versus system length (star: TE_{31}, circle: TE_{21}) and the time evolution of wave power (P_0) normalized to beam power (P_b) for $L = 5$ cm (b) peniotron interaction (TE_{31}) and (c) gyrotron interaction (TE_{21}).

The threshold of the absolute instability in an infinite system can be evaluated by using the expression derived in Ref. [19] which describes the spatial and temporal evolution of the response electric field to a localized initial disturbance

$$E(z,t) = \frac{1}{[2\pi i w''(k_0)t]^{1/2}} \times \exp\left[ik_0 z - iw(k_0)t + \frac{i(z - v_g t)^2}{2w''(k_0)t}\right], \quad (7)$$

where $\omega = \omega(k)$ is the dispersion relation for the peniotron interaction [14], ω_r and ω_i are the real and imaginary parts of ω, $v_g = \omega_r'(k_0)$ where k_0 is such that $w_i'(k_0) = 0$ and $w_i''(k_0) < 0$ and the prime is the derivative with respect to k_z. Note that two primes is the second derivative with respect to k_z. Equation (7) reveals that the evolving pulse peaks at $z = v_g t$, the pulse shape is growing and spreading in time if $\omega_i''(k_0)$ is negative, and its mean-square spatial spread is the reciprocal of $\mathrm{Im}[\frac{1}{w''(k_0)t}]$. The threshold can be determined from the fact that $E(z = 0, t)$ must increase exponentially with time or

$$\mathrm{Im}[w(k_0)] > \mathrm{Im}\left[\frac{v_g^2}{2\omega''(k_0)}\right], \quad (8)$$

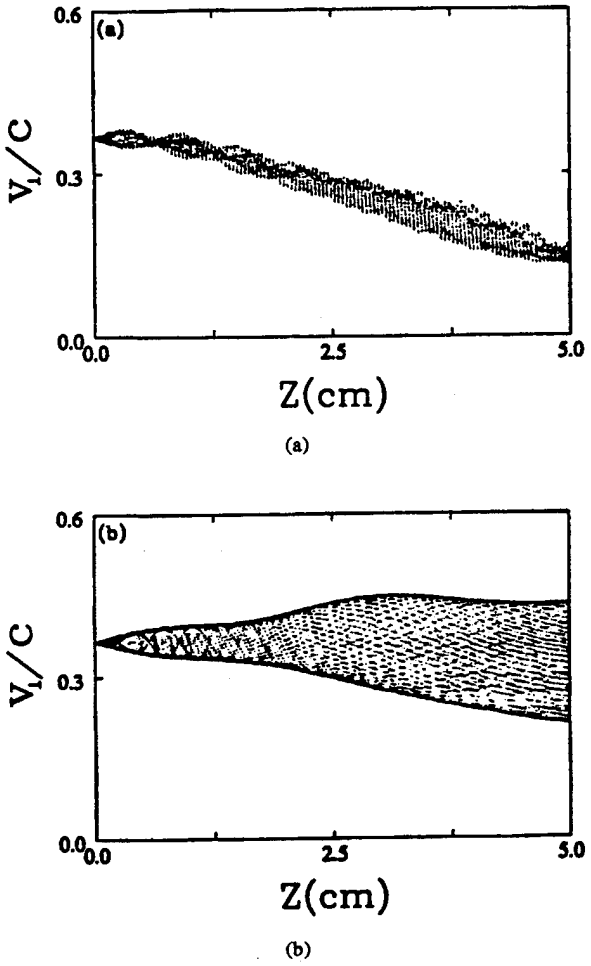

Fig. 3. Electron perpendicular velocity versus axial distance: (a) peniotron interaction and (b) gyrotron interaction.

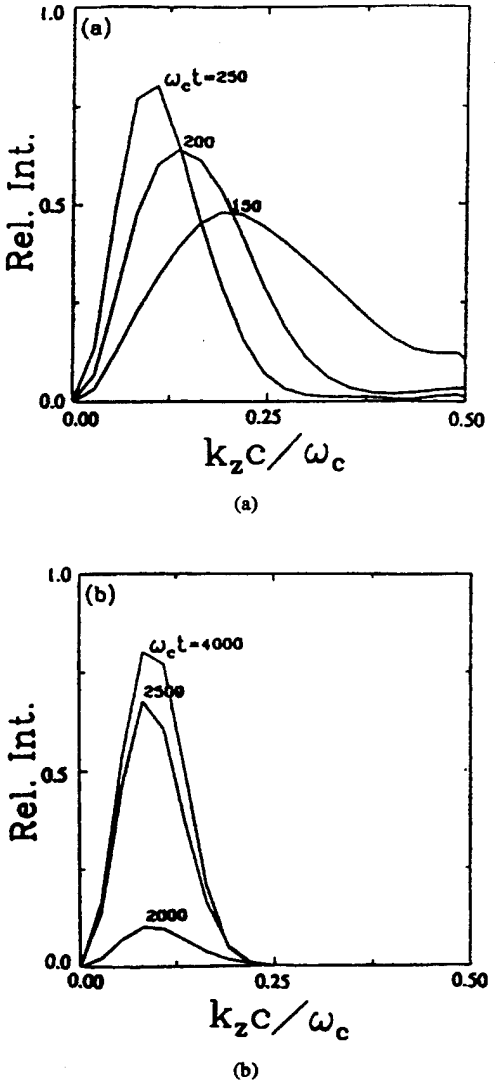

Fig. 4. Time evolution of the unstable k_z spectrum: (a) beforet he stored energy begins to grow and (b) during the growth.

This expression only gives an approximate threshold for self oscillation in an infinite system. By substituting the parameters used in the simulations into the dispersion relation given in Ref. [17], we obtained respectively $0.0157\omega_c$ for the left hand side and $0.014\omega_c$ for the right hand side of (8). Clearly, the inequality in (8) is satisfied. The evidence of spatial pulse spreading at early time can also be infered indirectly from Fig. 4(a) which displays the time evolution of an unstable pulse in wave number space before the stored energy begins to exponentiate in time. Notice that the pulse width in real and k_z space is inversely proportional to each other. The width of the unstable k_z spectrum remains relatively constant during the wave growing period (Fig. 4(b)). In carrying out a theoretical analysis [20] of absolute instability in cyclotron resonance masers, it is also found that a forward propagating wave is capable of giving rise to self-oscillation. However no physical mechanism is provided to explain the feedback mechanism. Here, we introduce a very rough intuitive argument of pulse spreading in an infinite system as the feedback mechanism. In a finite system, the temporal growth rate of the absolute instability depends on the strength of the feedback mechanism which partly depends on the total spatial gain of the most unstable mode. The effects of finite system length on the instability were demonstrated in the simulation but still remain to be investigated theoretically. As is known that an absolute instability grows from the initial fluctuation of the system eigenmodes and is eventually saturated by some nonlinear mechanism. Therefore by properly choosing the parameters one should be able to turn it into a useful microwave source. Based on our prelimary simulation results which will be presented later, the proposed mechanism possesses certain unique characteristics which make it a very attractive and viable peniotron microwave source.

To assure that the oscillation from the TE_{21} mode would not deteriorate the performance of the desired peniotron operation, multimode simulations were carried out. Fig. 5 shows the time evolution of the stored energy in the interaction space for three different cases. With $L = 5$ cm (Fig. 5(a)) the initial growth of the TE_{21} mode comes from the convective unstable mode with positive k_z and the growth rate of its absolute unstable mode is so small that it can be easily suppressed by the growth of the TE_{31} mode. Lengthening the system length to 8 cm tends to enhance the gyrotron interaction more than the peniotron interaction. In this case the two interactions have about the

same growth rate (Fig. 5(b)). The peniotron mode eventually is able to suppress the gyrotron mode. Using $L = 8$ cm and $I = 1.5$ A (Fig. 5(c)) the temporal growth rate of the gyrotron interaction now surpasses that of the peniotron interaction. However the peniotron interaction is still able to suppress the gyrotron interaction. The respective time evolution of the peniotron output power of the three cases described in Fig. 5 is shown in Fig. 6. Both single mode and two mode simulations are presented. The results indicate that the presence of the gyrotron interaction when it reaches large amplitude may affect the temporal growth rate of the peniotron interaction, which requires no phase bunching but not its final efficiency for all three cases. This is because a saturated gyrotron mode induces effective beam guiding center and velocity spreads to a peniotron interaction which would reduce the temporal growth rate. In principle, one should be able to derive two coupled nonlinear equations which govern the time evolution of the gyrotron and peniotron modes. Each equation should contain a linear gain term, a self-saturation term, and a cross-saturation term. The last term arises from the induced guiding center and velocity spreads by the other mode. In doing so, the time-dependent behavior of mode competition may be followed. Since at the end the gyrotron mode is completely suppressed and returns to its noise level, the peniotron mode should be able to attain the efficiency without the influence of the gyrotron mode. The effects of guiding center spread and beam current on the performance of the oscillator ($L = 5$ cm) are respectively displayed in Fig. 7(a) and Fig. 7(b). The results show that a 20 % guiding center spread would degrade the output efficiency to 40 % and $I = 3.5$ A is the optimal beam current for maximizing the effieciency. The optimal system length (L_0) which maximizes the output efficiency is very close to 5 cm ($I = 3.5$ A). With $L > L_0$, most of the electrons (in the $z > L_0$ region) are no longer axis encircling due to changes in their energy and guiding center location. These electrons eventually becomes resonance with the wave. As a result of detuning, electrons on the average start to absorb energy from the wave and terminate the wave growth process.

IV. Summary

In summary, we have proposed a scheme for establishing peniotron forward wave oscillator without external reflection. The feedback mechanism relies on the pulse spreading of the absolute instability. Simulation results also reveal that the peniotron interaction is capable of suppressing the gyrotron interaction. This suppression phenomenon should also occur in a conventional peniotron oscillator which requires less beam current to start the interaction.

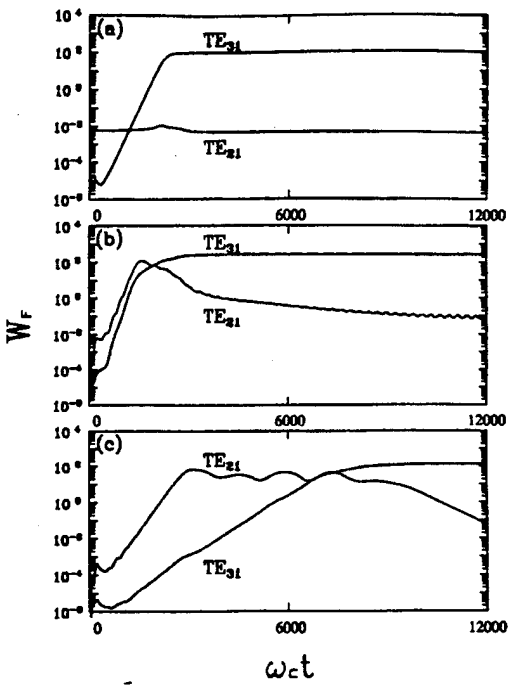

Fig. 5. Time evolution of normalized stored wave energy (W_f) from multi mode simulations. (a) $L = 5$ cm, $I = 3.5$ A, (b) $L = 8$ cm, $I = 3.5$ A, and (c) $L = 8$ cm, $I = 1.5$ A.

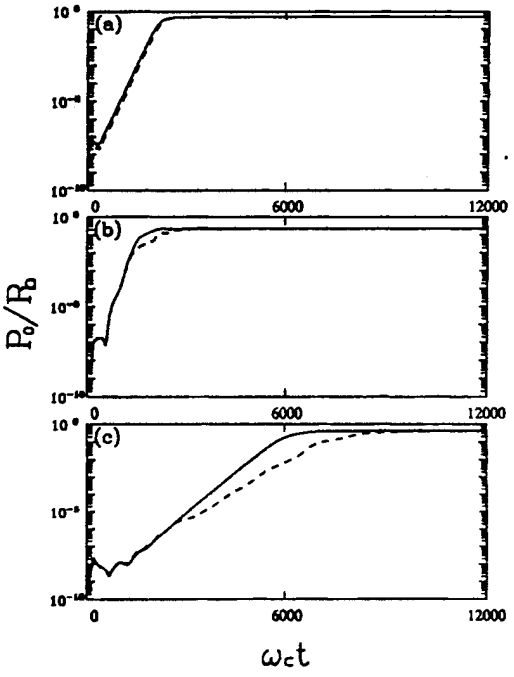

Fig. 6. Time evolution of peniotron output wave power (solid curve is from single mode simulation, dashed curve is from multi mode simulation: (a) $L = 5$ cm, $I = 3.5$ A, (b) $L = 8$ cm, $I = 3.5$ A, and (c) $L = 8$ cm, $I = 1.5$ A.

Acknowledgment

References

[1] K. Yamanouchi, S. Ono, and Y. Shibata, in *Proc. 5th Inter. Microwave Tube Conf.*, Paris, vol. 321, 1964.
[2] S. Ono, K. Tsutaki, and T. Kageynama, *Int. J. Electron*, vol. 56, p. 507, 1984.
[3] P. Vitello, *Int. J. of Infrared and Millimeter Waves*, vol. 8, p. 487, 1987.
[4] A. K. Ganguly, S. Ahn, and S. Y. Park, *Int. J. Electron*, vol. 65, p. 597, 1988.
[5] P. S. Rha, L. R. Barnett, J. M. Baird, and R. W. Grow, *IEEE Trans. on Electron Devices*, vol. 36, p. 789, 1989.
[6] G. Döhler, D. Gallagher, C. Lowrie, R. Moats, and F. Scafuri, in *Int. Electron Device Meeting*, p. 845, 1984.
[7] K. Yokoo, H. Shimawaki, H. Tadano, T. Ishihara, K. Sagae, N. Sato, and S. Ono, in *17th Int. Conf. on Infrared and Millimeter Waves*, p. 498, 1992.

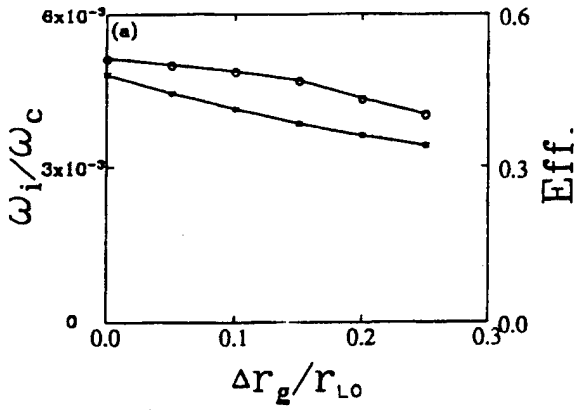

(a)

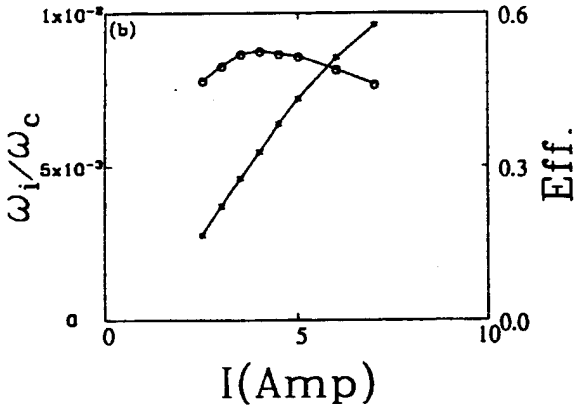

(b)

Fig. 7. Effects of (a) guiding center spread (Δ_{r_g} and r_{L_0} are respectively the inject beam guiding center spread and beam radial location) and (b) beam current on the performance of the oscillator (star: growth rate, circle: efficiency).

[8] G. S. Park, J. L. Hirshfield, R. H. Kyser, C. M. Armstrong, and A. K. Gauguly, in *17th Int. Conf. on Infrared and Millimeter Waves*, p. 500, 1992.

[9] Y. Y. Lau and L. R. Barnett, *Int. J. Infrared and Millimeter Waves*, vol. 3, p. 619, 1982.

[10] K. R. Chu and D. Dialetis, *Infrared and Millimeter Waves*, New York: Academic Press, vol. 13, no. 45, 1985.

[11] N. M. Kroll and E. L. Willis, *J. Appl. Phys.*, vol. 19, p. 166, 1947.

[12] T. H. Kho and A. T. Lin, *Nucl. Instruments and Methods in Phys. Res.*, vol. A296, p. 642, 1990.

[13] T. A. Spencer, R. M. Gilgenbach, and J. J. Choi, *J. Appl. Phys.*, vol. 72, p. 1221, 1992.

[14] C. S. Kou, S. H. Chen, L. R. Barnett, H. Y. Chen, and K. R. Chu, *Phys. Rev. Letts.*, vol. 70, p. 924, 1993.

[15] K. R. Chu and A. T. Lin, *IEEE Trans.-Plasma Sci.*, vol. 16, no. 90, 1988.

[16] J. A. Davis, *Phys. Fluids*, , vol. B1, no. 663, 1989.

[17] A. K. Ganguly, Y. Y. Lau, and S. Ahn, *Phys. Fluids*, , vol. B4, p. 3800, 1992.

[18] A. Bers, A. K. Ram, and G. Francis, *Phys. Rev. Lett.*,, vol. 53, p. 1457, 1984.

[19] T. Stix, "Waves in plasma," American Institute of Physics, 1992, ch. 9.

[20] J. A. Davis, R. C. Davidson, and G. L. Johnston, *IEEE Trans-Plasm Sci.*, , vol. 18, p. 286, 1990.

A. T. Lin, photograph and biography unavailable at time of publication.

Chih-Chien Lin, photograph and biography unavailable at time of publication.

APPENDIX 3

Slotted Third-Harmonic Peniotron Forward-Wave Oscillator

A.T. Lin,[b] C.K. Chong,[a] D.B. McDermott,[a] A.J. Balkcum,[a] F.V. Hartemann,[a] and N.C. Luhmann, Jr.[a]

[a]Department of Applied Science, University of California, Davis, CA 95616
[b]Department of Physics, University of California, Los Angeles, CA 90024

ABSTRACT

An experiment has been built to test the novel, efficient peniotron interaction at the third harmonic in a slotted eight-vane waveguide by using the axis-encircling electron beams produced by a gyroresonant rf accelerator. By configuring the oscillator so that the peniotron is excited as a forward wave at the cutoff frequency of a travelling-wave circuit, the peniotron can be made to dominate over the usually stronger gyrotron interaction. The 10 GHz peniotron will be driven by a 70 kV, 3.5 A axis-encircling electron beam with $\alpha = v_\perp/v_z = 1.3$ and is predicted by a nonlinear, self-consistent, multi-mode PIC code to yield 110 kW with 45% efficiency. The travelling-wave circuit is terminated on the upstream end by a load and by a transition to a TE_{41}/TE_{11} mode converter on the collector end. PIC code simulation results and a description of the assembled experiment are presented.

1. INTRODUCTION

Extensive efforts are underway to develop a high power, fast-wave 95 GHz amplifier.[1-5] The harmonic slotted peniotron travelling-wave tube[6] (peniotron-TWT) with an axis-encircling electron beam as shown in Fig. 1 is one approach that is being pursued because of its potential for high efficiency and lower magnetic field requirements. A slotted waveguide[7,8] is used to enhance a particular azimuthal mode and allows a low voltage electron beam to be used. Since the electrons interact with the rf fields fringing from the slot gaps, they should orbit fairly close to the vanes for strong interaction.

The peniotron's resonance condition is $\omega = (n\text{-}1)\Omega_c$ for the excitation of an n^{th}-order azimuthal mode with an axis-encircling beam. The peniotron interaction[6,9-14] is depicted in Fig. 2. Due to the isochronous resonance, in which the electrons fall back by one cycle during one gyro-orbit, the electrons experience the mode as a plane wave and $\underline{E}x\underline{B}$ drift towards the position where they are phased to lose energy. Due to the gradient in the rf field, deceleration dominates acceleration and gain results. Under the radial perturbation, the axis-encircling beam will form into n flutes. For an ideal beam, all electrons follow the same trajectory, except for a phase dependence which displaces the orbits in azimuth. All electrons will lose energy, resulting in extremely high efficiency. It has been observed in simulation[10] that the transfer of the beam's transverse energy can be as high as 99%.

The problem is that the peniotron interaction is weaker than the gyrotron interaction, and therefore, a peniotron will usually be suppressed by competing gyrotron modes. In the overmoded, slotted high-harmonic peniotrons currently under study, there are a multitude of intersections of the various cyclotron harmonic resonance lines with the many different waveguide modes, which can all lead to gyrotron oscillation. We have investigated a device in which the peniotron will dominate. This is achieved by exciting the peniotron in a travelling-wave circuit at the cutoff frequency.[15]

This paper is organized as follows. In Sec. 2, the problem of gyrotron mode competition in a peniotron is discussed. PIC code simulation results are presented for a case where the peniotron dominates and high efficiency results. An experiment that has been constructed to test this efficient, third-harmonic slotted peniotron is described in Sec. 3 and the summary is given in Sec. 4.

2. PENIOTRON/GYROTRON MODE COMPETITION

The dispersion diagram for a typical third-harmonic slotted peniotron-TWT is shown in Fig. 3. In order to achieve amplification, the third-harmonic cyclotron resonance line grazes the π mode of an eight-vane slotted waveguide. Unfortunately, the third-harmonic resonance line also intersects the $3\pi/4$ mode very close to the cutoff frequency, which will lead to third-harmonic gyrotron oscillation, especially since the gyrotron is a much stronger interaction. (Note: The mode designation, such as π or $3\pi/4$, specifies the phase shift of the wave between neighboring slots. Also, the π mode in an eight-vane waveguide is comprised of the azimuthal harmonics $m = 4, 12, 20, \ldots$ and the $3\pi/4$ includes $m = 3, 11, 19, \ldots$ and $m = 5, 13, 21, \ldots$) Another potential threat to the amplifier's stability is the intersection of the fourth-harmonic cyclotron resonance line with the π mode in the negative-k_z region, which is likely to result in a fourth-harmonic gyro-BWO interaction. In addition, the desired third-harmonic peniotron intersection itself can also lead to gyrotron interaction,

and potential dominance, if the electron beam's radial guiding-center spread is sufficiently large. By simulating this peniotron-TWT with a nonlinear, self-consistent, multi-mode particle-in-cell (PIC) code,[16,17] we found that the amplifier sections will oscillate as a gyrotron unless their lengths are extremely short. Unfortunately, an interaction section less than the critical oscillation length is too short for the peniotron amplifier to display sufficient gain.

We have developed an oscillator geometry where the peniotron interaction will dominate. The dispersion diagram for the new third-harmonic slotted peniotron oscillator is shown in Fig. 4. The third-harmonic cyclotron resonance line intersects the π mode of a terminated, nonresonant, slotted eight-vane waveguide at its cutoff frequency. Although there are again many potential harmonic gyrotron intersections as in Fig. 3, the third-harmonic peniotron will dominate due to the stronger interaction impedance that exists near cutoff. The intersection has been designed for positive k_z to excite a forward propagating wave. The required feedback for this oscillator is provided by pulse broadening.[18]

The PIC code, which can concurrently retain many modes (several hundred longitudinal modes for each of several transverse modes) and all types of interaction, was also used to investigate the travelling-wave peniotron interaction. For the parameters listed in Table I, a 70 kV, 3.5 A axis-encircling electron beam with $\alpha = v_\perp/v_z = 1.3$ is predicted to generate 110 kW at the third harmonic of the cyclotron frequency with an efficiency of 45% as shown in Fig. 5. Although this is an absolute instability, it is apparent that the excited wave is a forward-propagating wave since the rf power level is higher from the collector end. Figure 6 shows the behavior of the particle motion in the circuit. It is clear that this is a peniotron interaction since all electrons are decelerated. Gyrotron interactions have the signature that a fairly large fraction of the particles are accelerated.

3. DESCRIPTION OF EXPERIMENT

In order to test this novel, efficient oscillator, an experiment has been built for operation at 10 GHz. A schematic of the circuit is shown in Fig. 7. The parameters of the test oscillator are the same as were used in the simulation that yielded 45% efficiency (Table I). It is crucial that the interaction circuit be terminated on both ends so that it is nonresonant. In this way, interactions at the cutoff frequencies are emphasized. The travelling-wave circuit is terminated on the electron-source end by a load. The slotted load is created by placing tapered wedges of absorbing dielectric in each of the eight slots. The interaction region ends with a transition from the slotted structure to circular waveguide to convert the π mode into the TE_{41} mode, which is then transformed into the more useful TE_{11} mode in a four-period corrugated beat-wave mode converter[19] (see Fig. 8). The conversion efficiency of the TE_{41}/TE_{11} mode transformer is shown in Fig. 9. Finally, a circular to rectangular waveguide transition allows the output to be measured with standard waveguide components. The entire slotted X-band circuit has been fabricated by electric discharge wire machining. The individual circuit elements are bolted together into a vacuum chamber within the bore of a solenoid magnet.

Cusp electron guns[20] are the most appropriate source of axis-encircling electron beams for this device. However, they are currently under development and not yet available. Our gyroresonant rf accelerator[21,22] will be employed for producing the axis-encircling electron beams to test this novel peniotron oscillator. The third-harmonic peniotron experiment was designed so that the parameters of the electron beam are the same as in our current slotted third-harmonic gyrotron-TWT experiment.[23] The low-Q TE_{111} mode of the accelerator cavity is driven in circular polarization through two ports by a tunable 1 MW klystron amplifier. A 30 kV, 3.5 A electron beam from a scaled (x 3.5) SLAC 5045 klystron electron gun is injected along the magnetic field lines through an aperture into the accelerator cavity along the cavity's axis. The magnetic field is adjusted so that the electrons are gyroresonant with the wave. The measured acceleration characteristics of the 2.87 GHz cavity are shown in Fig. 10. Since this rf accelerator conserves the electrons' guiding-centers, the thickness of the output electron ring is equal to the diameter of the initial pencil electron beam.

4. SUMMARY

A new configuration has been proposed that ensures that the peniotron interaction will grow instead of a stronger gyrotron interaction. By arranging that the peniotron is excited at the cutoff frequency of a travelling-wave circuit, the peniotron can be made to dominate over the usually prevalent gyrotron. A PIC simulation code predicts that the new oscillator driven by a 70 kV, 3.5 A, $\alpha = 1.3$ axis-encircling electron beam will generate a 110 kW forward-wave at the third harmonic with an efficiency of 45%. An experiment has been described that was built to test this novel, efficient, third-harmonic peniotron interaction at 10 GHz in a slotted, eight-vane waveguide by using the axis-encircling electron beams produced by our gyroresonant rf accelerator. The travelling-wave circuit is terminated on the upstream end by a load and by a transition to a TE_{41}/TE_{11} mode converter on the collector end.

After this novel interaction has been successfully tested and optimized in this proof-of-principle experiment, higher frequency peniotrons will be built which would employ the newly developed cusp guns.

This work has been supported by the U.S. AFOSR under Grants 91-0382, F49620-93-1-0628, F49620-92-J-0175, and Rome Laboratory (ATRI) under Contract F30602-91-C-0020.

REFERENCES

(1) W. DeHope, G. Hu, M. Mizuhara, J. Neilson, R. Schumacher, C. Chong, A. Lin, N. Luhmann, Jr., D. McDermott, and T. Stewart, "Design and Development of a Third-Harmonic, 95 GHz Gyro-TWT," in *Tech. Dig. of IEEE Int. Electron Dev. Meet. (IEDM)*, pp. 203-206, 1992.
(2) G.S. Park, J.L. Hirshfield, R.H. Kyser, C.M. Armstrong and A.K. Ganguly, "35 GHz Gyro-Peniotron Amplifier Experiment," in *Digest of Int. Conf. on Infrared and Millimeter Waves*," pp. 500-501, 1992.
(3) S. Begum, G. Scheitrum, and B. Arfin, "Large Signal Simulation and Design of a 95 GHz Harmonic Gyroklystron Amplifier," in *Tech. Dig. of IEEE Int. Electron Dev. Meet. (IEDM)*, pp. 199-202, 1992.
(4) G. Dohler, D. Gallagher, J. Richards, and F. Scafuri, "Harmonic High Power 95 GHz Peniotron," in *Tech. Dig. of IEEE Int. Electron Dev. Meet. (IEDM)*, pp. 363-366, 1993.
(5) C.K. Chong, D.B. McDermott, A.T. Balkcum, N.C. Luhmann, Jr., "Nonlinear Analysis of High-Harmonic Slotted Gyro-TWT Amplifier," *IEEE Trans. on Plasma Science*, vol. **20**, no. 3, pp. 176-87, 1992.
(6) A.K. Ganguly, S. Ahn and S. Y. Park, "Three Dimensional Nonlinear Theory of the Gyropeniotron Amplifier," *Int. J. Electron.* **65**, 597 (1988).
(7) Y.Y. Lau and L.R. Barnett, "Theory of a Low Magnetic Field Gyrotron (Gyromagnetron)," *Int. J. Infrared and Millimeter Waves*, vol. **3**, no. 5, pp. 619-643, 1982.
(8) K.R. Chu and D. Dialetis, "Kinetic Theory of Harmonic Gyrotron Oscillation with Slotted Resonant Structure," in Infrared and Millimeter Waves, vol. **13**, New York Academic Press, pp. 45-75, 1985.
(9) S. Ono, K. Tsutaki, and T. Kageynama, *Int. J. Electron.* **56**, 507 (1984).
(10) P. Vitello, *Int. J. of Infrared and Millimeter Waves* **65**, 487 (1987).
(11) A.K. Ganguly, S. Ahn, and S.Y. Park, *Int. J. Electron.* **65**, 597 (1988).
(12) P.S. Rha, L.R. Barnett, J.M. Baird, and R.W. Grow, *IEEE Trans. on Electron Devices* **36**, 789 (1989).
(13) G. Dohler, D. Gallagher, C. Lowrie, R. Moats, and F. Scafuri, in *Tech. Dig. of IEEE Int. Electron Device Meeting (IEDM)*, 845 (1984).
(14) K. Yokoo, H. Shimawaki, H. Tadano, T. Ishihara, K. Sagae, N. Sato, and S. Ono, *Digest of Int. Conf. on Infrared and Millimeter Waves*, 500 (1992).
(15) A.T. Lin and C.C. Lin, "Peniotron Oscillators without Cavity Structures," submitted to *Appl. Phys. Lett.*, 1993.
(16) J.M. Dawson and A.T. Lin, Basic Plasma Physics, vol. II, ch. 7, M.N. Rosenbluth and R.Z. Sagdeev, Eds., North Holland, Amsterdam, The Netherlands, 1984.
(17. A.T. Lin, M. Caplan, and K.R. Chu, "A Study of Saturated Output of a TE_{01} Gyrotron Using an Electromagnetic Finite Size Particle Code," *Int. J. Electron.*, vol. **53**, p. 659, 1982.
(18) T.H. Stix, Waves in Plasmas, ch. 9, American Institute of Physics, New York, NY, 1992.
(19) C. Moeller, "Mode Converters Used in the Doublet III ECH Microwave System," *Int. J. Electron.*, vol. **53**, no. 6, pp. 587-593, 1982.
(20) N.R. Vanderplaats, H.E. Brown, and S. Ahn, "Magnetically Shielded Electron Guns with a Center Magnetic Post," in *Tech. Dig. of IEEE Int. Electron Dev. Meet. (IEDM)*, pp. 336-338, 1981.
(21) H.R. Jory and A.W. Trivelpiece, "Charged-Particle Motion in Large-Amplitude Electromagnetic Fields," *J. Appl. Physics*, vol. **39**, p. 3053-60, 1968.
(22) D.B. McDermott, D.S. Furuno and N. C. Luhmann, Jr., "Production of Relativistic, Rotating Electron Beams by Gyroresonant RF Acceleration in a TE_{111} Cavity," *J. Appl. Phys.* **58**, 4501 (1985).
(23) C.K. Chong, D.B. McDermott, A.T. Lin, W. DeHope, A.J. Balkcum, and N.C. Luhmann, Jr., "Scaled Tests of Varian's 95 GHz Slotted Third-Harmonic Gyro-TWT Amplifier," in this Proceedings.

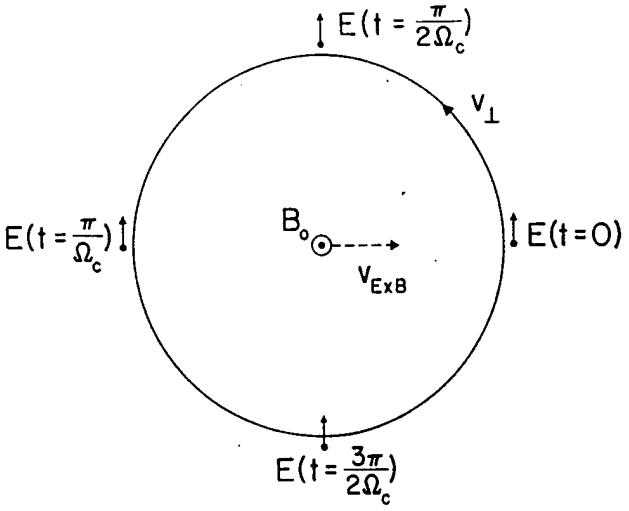

Fig. 1. Schematic of the asynchronous peniotron interaction with an axis-encircling electron beam and showing the orientation of the electric field at several positions of an electron's orbit.

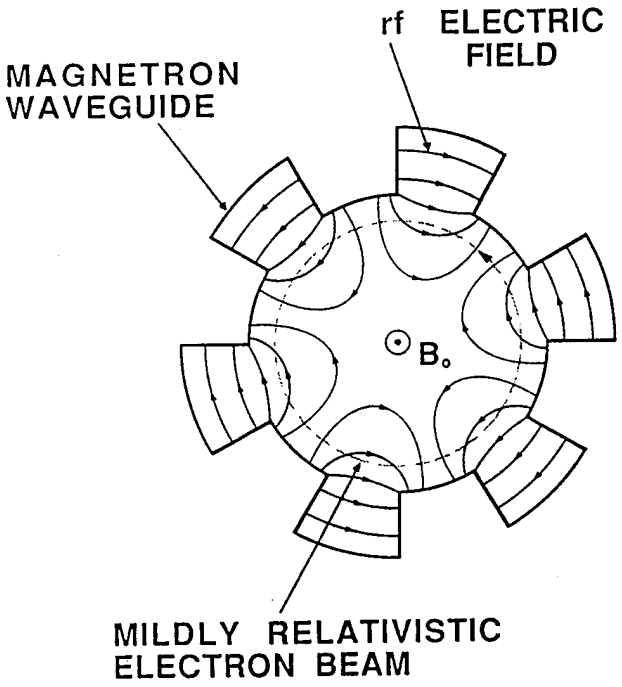

Fig. 2. Cross-sectional view of slotted second-harmonic peniotron-TWT with six vanes and showing the rf electric field pattern of the π mode.

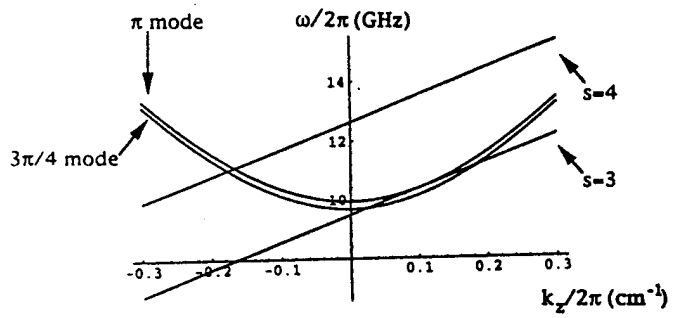

Fig. 3. Uncoupled dispersion relation of a third-harmonic slotted peniotron-TWT showing the third and fourth cyclotron harmonic resonance lines, the operating π mode and spurious 3π/4 mode.

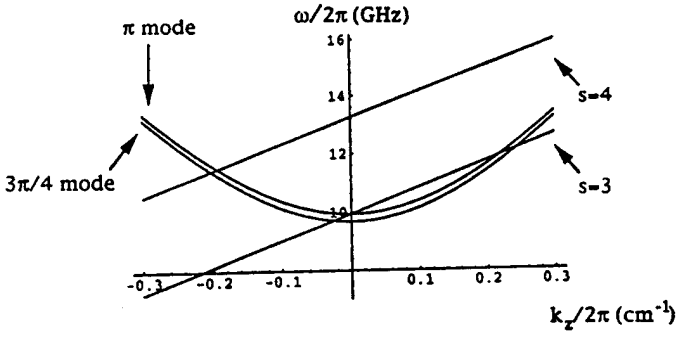

Fig. 4. Uncoupled dispersion relation of a third-harmonic slotted peniotron forward-wave oscillator showing the third and fourth cyclotron harmonic resonance lines, the operating π mode and spurious 3π/4 mode.

Table I Design Parameters for the 10 GHz, Slotted, Third-Harmonic Peniotron, Forward-Wave Oscillator.

Beam Voltage	70 kV
Beam Current	3.5 A
α ($v_\perp/v_z$)	1.3
Magnetic Field	1.3 kG
Cyclotron Harmonic	Third
Mode	π
Number of Vanes	8
$\omega_c/2\pi$	9.94 GHz
r_L/a	0.7
r_c/a	0.0
$\Delta r_c/a$	0.2
Inner Circuit Radius, *a*	0.800 cm
Outer Circuit Radius, *b*	1.296 cm
Interaction Length	20.3 cm

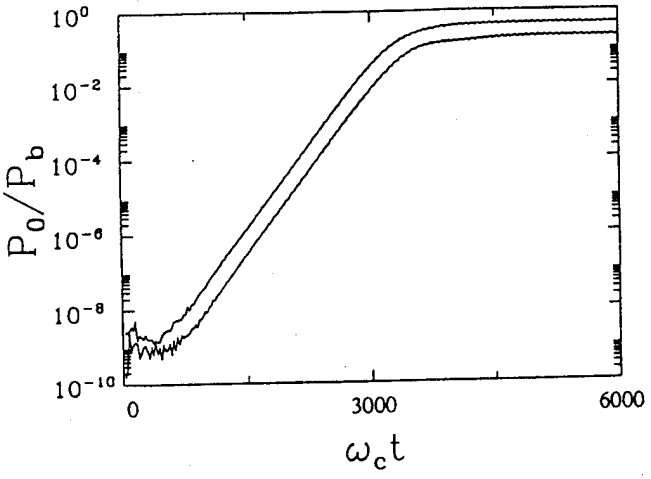

Fig. 5. Temporal dependence of third-harmonic peniotron's output power normalized to the beam power (Table I).

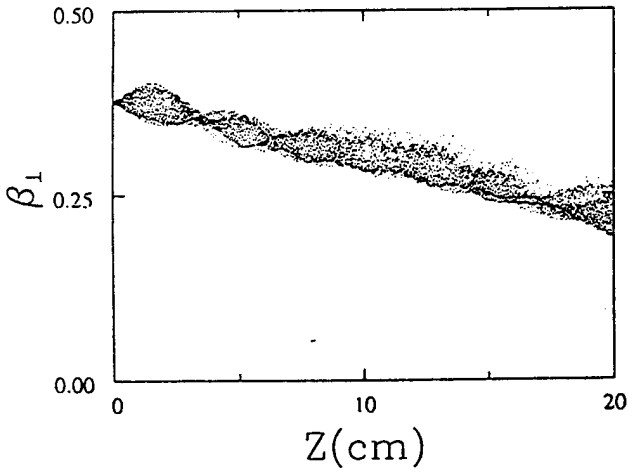

Fig. 6. Spatial dependence of transverse velocity in third-harmonic peniotron during saturation at $\Omega_c t = 4000$ (Table I).

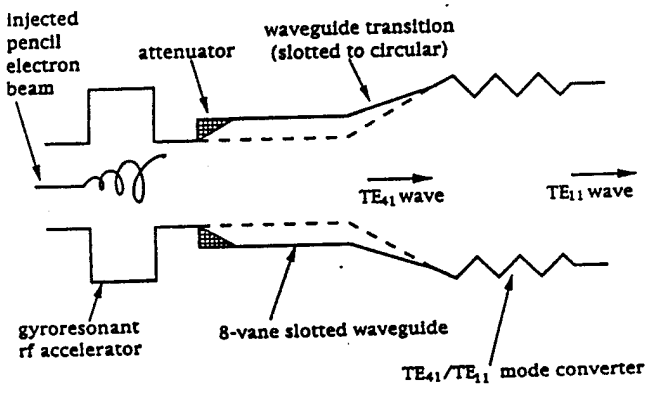

Fig. 7. Schematic of slotted third-harmonic peniotron forward-wave oscillator proof-of-principle experiment.

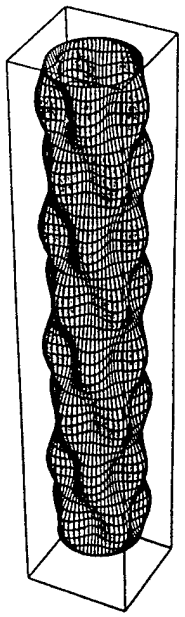

Fig. 8. Schematic of four-period TE_{41}/TE_{11} beat-wave mode converter.

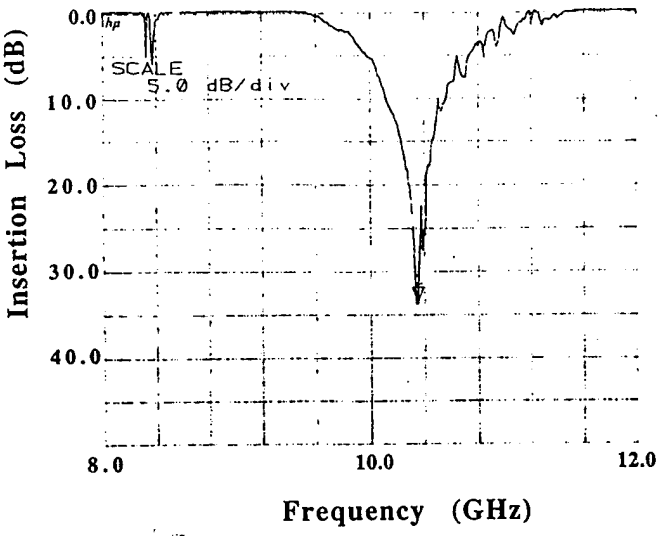

Fig. 9. Bandwidth measurement from network analysis of power remaining in TE_{11} mode for TE_{11} wave injected into four-period TE_{41}/TE_{11} beat-wave mode converter.

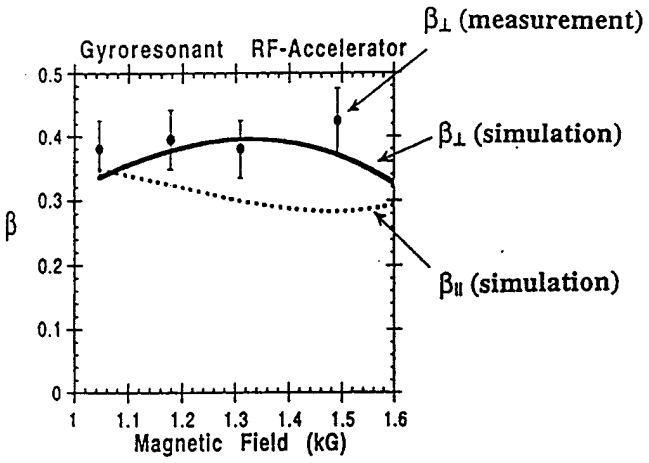

Fig. 10. Dependence on magnetic field of transverse and axial velocity (normalized to the speed of light) from gyroresonant rf accelerator with $P_{in} = 1$ MW and $L/r_W = 0.92$ from simulation (curves) and measurement (filled circles).

APPENDIX 4

Pulsating mode in peniotron backward wave oscillations

A. T. Lin and Chih-Chien Lin
Department of Physics, University of California at Los Angeles, Los Angeles, California 90024-1547

(Received 2 May 1994; accepted 26 July 1994)

A sustainable pulsating mode in peniotron backward wave oscillations can be excited if parameters are properly chosen, such that at some instant of time the reduction in beam energy resulting from the electron–wave interaction is to such an extent that its cyclotron harmonic line intersects with the waveguide dispersion curve in the positive k_z region. The generation of the forward traveling self-oscillating mode eliminates the residual backward traveling wave, which is very essential in establishing relaxation oscillation. As a result, the time evolution of the output wave becomes self-pulsating. © *1994 American Institute of Physics.*

I. INTRODUCTION

Coherent microwave generation based on the concept of the peniotron interaction was conceived[1] almost three decades ago. Since then, a great deal of theoretical effort,[2–5] which employed different electron beam and waveguide configurations has been devoted to predicting the performance of a peniotron device. All the calculations have shown that high efficiency at high cyclotron harmonic interaction is attainable. However, experiments carried out so far[6,7] have failed to provide convincing evidence to support that the promised high performance has been realized. From the past investigations, it is recognized that the essential elements of a high efficiency peniotron are a good quality axis-encircling electron beam and vaned waveguide. Recently based on these configurations, a high quality factor peniotron oscillator experiment,[7] third harmonic peniotron amplifier design,[8] and particle-in-cell simulations[9] to demonstrate the feasibility of building a forward wave peniotron oscillator without cavity structures, have been performed. It is hoped that the advance in the technology of producing high quality axis-encircling beams may eventually render high performance peniotrons achievable.

One of the unavoidable features of a vaned waveguide is the close frequency spacing of adjacent high-order modes. As was shown[9] the same beam cyclotron harmonic line that gives rise to the desired peniotron interaction is capable of exciting the gyrotron interaction of the adjacent mode. It is important to address the mode competition issue and determine which mode will survive in the nonlinear stage. In an oscillator configuration, it was illustrated[9] that regardless of their linear electron–wave coupling strength, the peniotron interaction always overwhelms gyrotron interaction if one waits a long enough time. This is because the latter is a resonance interaction that results in only a guiding center spread, but not a guiding center drift. Therefore, a saturated gyrotron mode will most likely only reduce the temporal growth rate of a peniotron mode, but not its efficiency. This observation may give sufficient confidence to experimentalists[7] to claim that their results indeed come from the peniotron interaction.

It has been recently shown[10–12] that the gyrotron backward wave oscillator is a high efficiency tunable microwave source. In this paper, we shall investigate the performance of peniotron backward wave oscillations to see whether they are able to attain the same efficiency level of their counterpart[9] (forward wave oscillator). In carrying out particle simulations we found that with proper choice of parameters, a peniotron backward wave oscillator can be operated in a sustained pulsating mode, with almost 90% modulation.

II. DISPERSION RELATIONS

In order to elucidate the physical mechanism responsible for sustaining the pulsating mode in peniotron backward wave oscillations, it is important to start with the dispersion relation in a configuration of an axis-circling electron beam propagating in a vaned waveguide. The result should exhibit the potential mode of interaction. A cylindrical waveguide slotted periodically around the circumference can be designed in such a way as to enhance a particular harmonic field component by rippling its RF field line, and is suitable for the high harmonic peniotron interaction. The cross-sectional view of a six vane slotted waveguide with an axis-encircling beam is displayed in Fig. 1(a). In the interaction region, the electric and magnetic fields of a transverse electric field mode[13,14] may be written as

$$E_n = E_{Tn}(z,t)(\hat{z}\times\nabla_\perp C_n), \tag{1}$$

$$B_n = B_{Tn}(z,t)\nabla_\perp C_n + \hat{z}B_{Ln}k_\perp C_n, \tag{2}$$

where C_n is the local wave function inside the inner radius ($r<a$)

$$C_n = -\sum_{m=-\infty}^{\infty} \frac{A_\Gamma}{k_\perp} J_\Gamma(k_\perp r)e^{j\Gamma\theta}. \tag{3}$$

Here $\Gamma = n+mN$, $n=0, 1,..., N-1$, m is any integer, N is the number of vanes, and $A_\Gamma = (N\theta_0/\pi)(\sin\Gamma\theta_0/\Gamma\theta_0)$ is the enhancement factor of the slotted structure. $k_\perp$ is the cutoff wave number, which can be determined from the circuit dispersion relation,

$$\sum_\Gamma \frac{J_\Gamma(k_\perp a)}{J'_\Gamma(k_\perp a)}\left(\frac{\sin\Gamma\theta_0}{\Gamma\theta_0}\right)^2 = -\frac{\pi}{N\theta_0}\frac{Z_0(k_\perp a)}{Z_1(k_\perp a)}, \tag{4}$$

where Z_Γ is a combination of Bessel function (J_Γ) and Neumann function (N_Γ) of order Γ,

 1070-664X/94/1(12)/1/5/$6.00

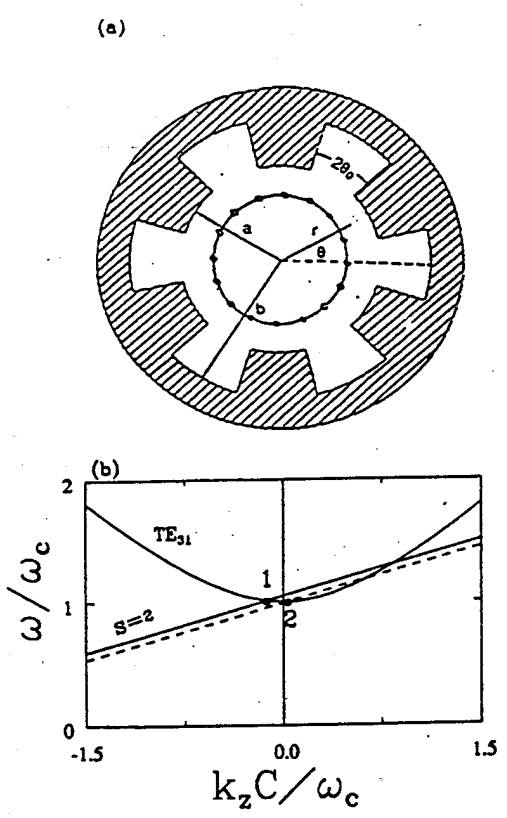

FIG. 1. Six vane slotted waveguide and an axis encircling beam: (a) cross-sectional view and (b) dispersion curves.

$$Z_\Gamma(x)=J_\Gamma(x)-\frac{J_1(k_\perp b)}{N_1(k_\perp b)}N_\Gamma(x), \tag{5}$$

and $\theta_0=2\pi/4N$. Here a and b denote, respectively, the inner and outer circuit radius. For each value of n, there are an infinite number of solutions from Eq. (4). The first root is the most important one, and the associated mode is usually designated by TE_{n1}. The mode number n is also the number of times the RF field pattern repeats in one rotation around the waveguide axis. There are many possible modes, but the two most interesting cases are the π mode, where adjacent slots are out of phase by π, and the 2π mode, where the phase in each slot is identical. In the most rigorous description, an infinite superposition of different Γ's to satisfy the vane boundary condition is required to represent each n mode. However, in most of the cases, an adequate approximation includes just two partial waves—those with $\Gamma=n$ and $(n-N)$. The physical meaning of this is that an electromagnetic wave rotating in a periodic structure must interfere with other waves to reproduce the static periodic pattern of the structure.

The modes supported by the slotted structure can interact with an axis-encircling electron beam through the relativistic gyrotron and nonrelativistic peniotron mechanisms. In a gyrotron interaction, it is necessary that an electron stays approximately in the same phase with respect to the wave as it traverses through the interaction region, so that the cumulative electron–wave interaction produces a substantial bunching through the relativistic mass effect. As a consequence, an initially randomly phased electron beam would end up with some of its electrons giving up energy to and the rest of them absorbing energy from the same wave. This resonant condition can be expressed as

TABLE I. Second harmonic vaned peniotron backward wave oscillator design.

Beam voltage	70 kV
Beam current	3.5 A
Mode	π mode
Number of vanes	6
$\alpha=v_\perp/v_\parallel$	1.2
Interaction length (L)	6 cm
$\omega_c/2\pi$	33.65 GHz
Inner circuit radius (a)	0.16 cm
Outer circuit radius (b)	0.304 cm

$$\omega_0=k_z v_z+s\frac{\Omega_c}{\gamma}, \tag{6}$$

where ω_0 and k_z are, respectively, the wave frequency and axial wave number. Here v_z and γ are the electron axial velocity and relativistic factor. In addition, Ω_c is the nonrelativistic cyclotron frequency and s is the harmonic number. For an efficient gyrotron interaction, n must be equal to s. On the other hand, the peniotron interaction requires $n=s+1$, which ensures that initially electrons periodically change their RF phase, such as to be alternatively accelerated and decelerated along their trajectories. At the same time, the same condition also gives rise to the electron guiding center drift, which couples with the positive radial RF field gradient in a vaned structure and provides the gain mechanism for the peniotron interaction. As a result, all electrons, regardless of their initial phases relative to the wave, convert their kinetic energy into wave energy. This makes peniotron devices inherently high efficiency.

An unavoidable feature of a vaned waveguide is the small-frequency separation between the modes of larger n, which renders the mode competition in peniotron devices an important issue to be addressed. Using the parameters of Table I the dispersion curves of the relevant waveguide mode (TE_{31}) and the second ($s=2$) cyclotron harmonic line are shown in Fig. 1(b) as solid curves. The potential peniotron backward wave oscillation, which relies on the backward propagating electromagnetic wave to feedback the energy generated by the forward propagating beam, is marked by point 1. The potential gyrotron backward wave oscillations are not shown here, since they could be suppressed by the growth of the peniotron mode.[9]

III. SIMULATION RESULTS

The cutoff wave number in the particle-in-cell code described in Ref. 14 is replaced by the value evaluated from Eq. (4), and the modified version has been utilized to simulate the nonlinear evolution of a peniotron backward wave oscillation. In the simulation, the electrons are continuously injected at $z=0$ with prescribed parameters, and are collected at $z=L$. Initially, the axis-encircling electrons fill up the in-

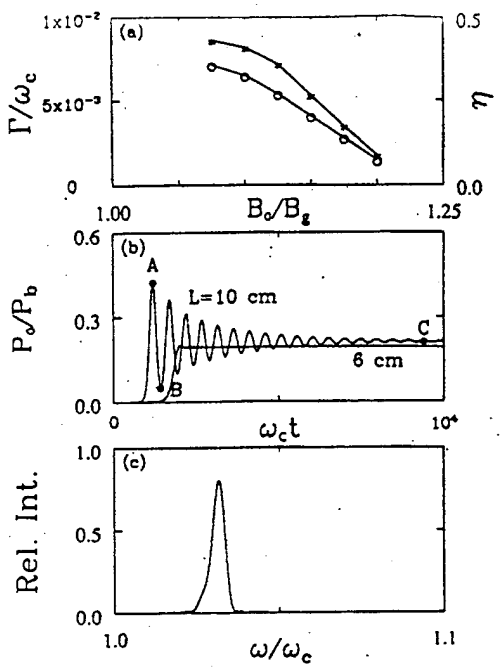

FIG. 2. Device performance: (a) efficiency η (circles) and growth rate Γ (stars) versus the magnetic field; (b) time evolution of output power for $B_0=1.15B_g$; and (c) output frequency spectrum ($L=6$ cm).

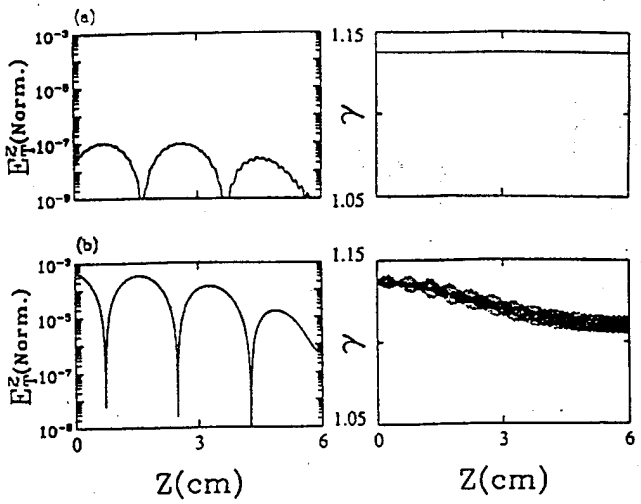

FIG. 3. Spatial distribution of electric field and beam energy ($L=6$ cm, $B_0=1.15B_g$; (a) $\omega_c t=10^3$ and (b) $\omega_c t=10^4$.

teraction region uniformly along the z direction. Resistive layers are provided on both sides of the interaction region to absorb the outgoing electromagnetic wave. In order to investigate the dependence of its output efficiency (η) and temporal growth rate (Γ) on the applied magnetic field (B_0), B_0 is varied from $1.075B_g$ to $1.2B_g$, where B_g is for grazing intersection ($\Omega_g=\gamma_0\omega_c/s\gamma_{z0}$, ω_c is the waveguide cutoff frequency). The simulation results are shown in Fig. 2(a), which reveals that both η and Γ tend to increase when B_0 decreases. This is because that the reduction in B_0 slows down the group velocity of the backward propagating electromagnetic wave, which prolongs its interaction with the electron beam. The increase in growth rate generally tends to enhance the output efficiency when the system length is below the saturation length. Figure 2(b) displays the time evolution of the output power at $z=0$ for the cases of $L=6$ and 10 cm ($B_0=1.15B_g$). In the shorter length case, the output wave grows from an initial noise signal, and saturates at about 20% efficiency. Its frequency spectrum [Fig. 2(c)] peaks at $\omega_0=1.032\omega_c$, which is at the proper frequency of point 1 in Fig. 1(b). When the length is above the critical oscillation length, the output power builds up in time because of the intrinsic positive feedback until a stable operating point is reached, which is determined by nonlinear effects in the beam kinematics. The positive feedback (gain) arises from the fact that the electromagnetic wave is in synchronism with the beam along the longitudinal direction, so that the backward travel wave energy contributions add in phase from successive locations. Consequently, the wave propagates from $z=L$ to $z=0$ is amplified at the expense of beam kinetic energy, and it imparts a perturbation to incoming beam electrons at the proper phase. The perturbed electrons traveled to the right emit wave that is in phase with the backward propagating wave from the right. The returned wave energy produces further perturbation, which, in turn, produces more returned energy. This regenerative process gives rise to the temporal growth of the output power, and the growth rate will be linear as long as the electron–wave interaction remains weak. When the wave amplitude increases to such an extent that the electron-wave interaction become nonlinear and the longitudinal synchronism is detuned, gain saturation will occur, and eventually a steady state is reached. If the system length is only slightly longer than the critical oscillation length, the transition from the growth state to the steady state is rather smooth. The spatial distribution of the wave intensity and the electron relativistic factor at $\omega_c t=10^3$ (linear regime) and $\omega_c t=10^4$ (steady state) are shown, respectively, in Figs. 3(a) and 3(b). The wave intensity exhibits an exponentially spatial growth along the backward direction at both instants of time. The electron kinetic energy is hardly affected by the wave in the linear regime, while it is substantially reduced along the forward direction in the nonlinear regime. Notice that in the latter case, the electron–wave energy exchange has yet to reach saturation at $z=L$.

When the interaction length is increased to 10 cm, which far exceeded the critical oscillation length, the gain is much stronger than the previous case. As a consequence, the output power overshoots its steady-state level [Fig. 2(b), point A], and as a result the electron–wave energy exchange terminates at a distance less than that of the steady-state value. This renders the gain for the backward traveling wave insufficient to sustain the overshot output power, which then drops to below the steady-state level [Fig. 2(b), point B]. At this wave intensity level, the electron beam is again capable of generating enough gain to maintain the output power growth. This process will repeat itself periodically, but each time the residual wave intensity level will become closer to the steady-state level [Figs. 2(b), point C]. In the steady state, the effective interaction length where electrons convert their energy into wave energy is substantially reduced from

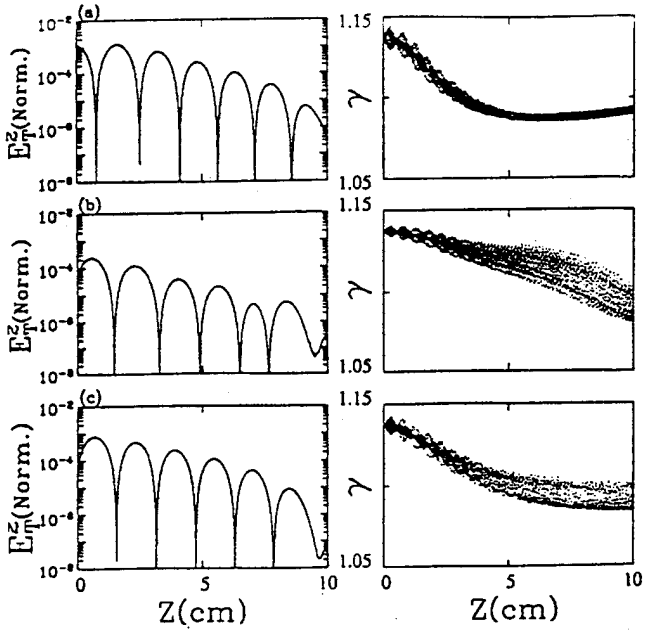

FIG. 4. Spatial distribution of electric field and beam energy at three instants of time of Fig. 2(b), (a) corresponding to point A, (b) corresponding to point B, and (c) corresponding to point C.

the original system length. This entire process results in the relaxation oscillation in the output wave time evolution. The above argument is illustrated in Fig. 4, which shows the spatial distribution of the wave intensity and the electron relativistic factor at three instants of time, corresponding to points A, B, and C in Fig. 2(b).

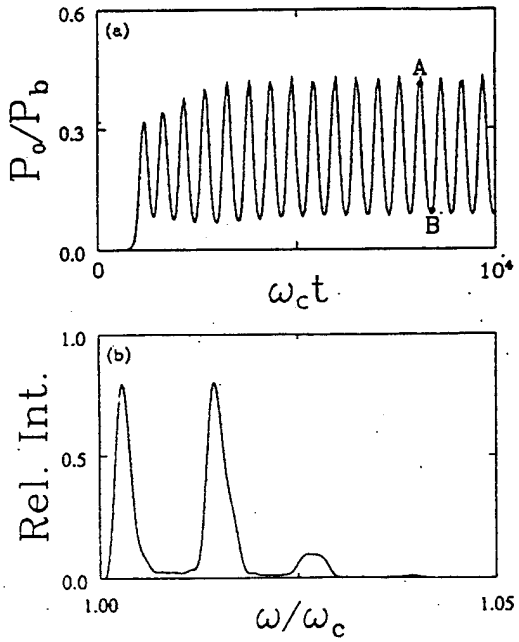

FIG. 5. Pulsating mode using $B_0=1.1B_g$ and $L=7$ cm: (a) time evolution of output power and (b) output frequency spectrum.

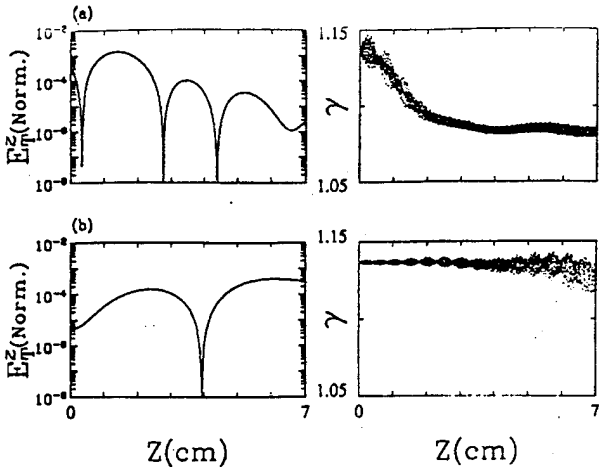

FIG. 6. Spatial distribution of the electric field and beam energy at two instants of time of Fig. 5(a): (a) corresponding to Point A and (b) corresponding to point B.

Lowering the applied magnetic field to $B_0=1.1B_g$ ($L=6$ cm) increases the growth rate, but the output power still exhibits relaxation oscillation. If, at the same time, the interaction length is increased to 7 cm, the time evolution of the output power is drastically changed from the previous case. Figure 5(a) shows the time history of the output power at $z=0$. A sustained pulsation is clearly observed. Figure 5(b) displays the electric field frequency spectrum analysis taken at $z=0$, which consists of two different components corresponding to points 1 and 2 in Fig. 1(b). In order to elucidate the physical mechanism, which gives rise to the generation of this new mode, the spatial distribution of the wave intensity and the electron relativistic factor corresponding to the peak and valley of the pulsating oscillation is shown in Fig. 6. The simulation results reveal that at the instant of peak wave intensity [Fig. 6(a)], the effective interaction length is drastically shortened, which produces a lower-energy beam ($\gamma \simeq 1.08$) in the upstream region. If this beam energy is used to draw the electron harmonic cyclotron line, which is shown as a dotted line in Fig. 1(b), its intersection with the waveguide dispersion curve is clearly in the positive k_z region. This is a potential source of self-oscillation, and its excitation is supported by examining Fig. 6(b), which demonstrates that the wave indeed propagates in the forward direction. The generation of this forward propagating oscillation eliminates the residual backward propagating wave and prevents the output wave from attaining the steady-state level. If the applied magnetic field B_0 is reduced to $1.05B_g$, the pulsating mode disappears, and the relaxation oscillation is again observed. This is because, in this case, the electron harmonic cyclotron line evaluated at the peak intensity is below the waveguide dispersion curve.

IV. SUMMARY

In carrying out computer simulations of peniotron backward wave oscillations, a sustainable self-pulsating mode is observed if the parameters are properly chosen. This new

mode of operation can only be established if, at some instant of time, the electron beam energy is reduced to such an extent that its cyclotron harmonic line intersects the waveguide curve in the positive k_z region. The generation of a self-oscillating forward traveling mode diminishes the residual backward traveling wave and keeps the system from reaching the steady state.

ACKNOWLEDGMENT

This work was supported by the Air Force Office of Scientific Research under Grant No. F49620-93-1-0628 and the San Diego Supercomputing Center.

[1]K. Yamanouchi, S. Ono, and Y. Shibata, *Proceedings of the 5th International Microwave Tube Conference*, Paris (Academic, London, 1964), p. 321.
[2]S. Ono, K. Tsutaki, and T. Kageynama, Int. J. Electron. **56**, 507 (1984).
[3]P. Vitello, Int. J. Infrared Millimeter Waves **8**, 487 (1987).
[4]A. K. Ganguly, S. Ahn, and S. Y. Park, Int. J. Electron. **65**, 597 (1988).
[5]P. S. Rha, L. R. Barnett, J. M. Baird, and R. W. Grow, IEEE Trans. Electron. Devices ED-36, 789 (1989).
[6]G. Döhler, D. Gallagher, C. Lowrie, R. Moats, and F. Scafuri, *International Electronic Device Meeting*, Technical Digest, San Francisco, 1984 (Institute of Electrical and Electronic Engineering, New York, 1984), p. 845.
[7]K. Yokoo, H. Shimawaki, H. Tadano, T. Ishihara, K. Sagae, N. Sato, and S. Ono, *17th International Conference on Infrared and Millimeter Waves*, Pasadena, CA, 1992 (SPIE, Bellingham, WA, 1992), p. 498.
[8]G. S. Park, J. L. Hirshfield, R. H. Kyser, C. M. Armstrong, and A. K. Gauguly, in Ref. 7, p. 500.
[9]A. T. Lin and C-C. Lin, Appl. Phys. Lett. **64**, 1088 (1994).
[10]T. A. Spencer, R. M. Gilgenbach, and J. J. Choi, J. Appl. Phys. **72**, 1221 (1992).
[11]C. S. Kou, S. H. Chen, L. R. Barnett, H. Y. Chen, and K. R. Chu, Phys. Rev. Lett. **70**, 924 (1993).
[12]A. T. Lin and C-C. Lin, Phys. Fluids B **5**, 2314 (1993).
[13]K. R. Chu and D. Dialetis, *Infrared and Millimeter Waves* (Academic, New York, (1985), Vol. 13, p. 45.
[14]T. H. Kho and A. T. Lin, Nucl. Instrum. Methods Phys. Res. A **296**, 642 (1990).